University of Stavanger

Faculty of Science and Technology

MASTER'S THESIS

Study program/Specialization: Petroleum Geosciences Engineering	\<Spring, 2016\> Open
Writer: Bilal Ahmed Bhatti	 _____ (Writer's signature)

Faculty supervisor: R. James Brown External supervisor(s): Børge Rosland

Title of thesis: Low-frequency seismic analysis and direct hydrocarbon indicators

Credits (ECTS): 30

Keywords: Low-frequency Spectral decomposition Direct hydrocarbon indicators Homogeneity and heterogeneity Reservoir characterization	Pages: 78 +enclosure: CD Stavanger, 15th June, 2016

Low frequency seismic analysis and direct hydrocarbon indicators

by

Bilal Ahmed Bhatti, B. Sc.

Thesis

Presented to the Faculty of Science and Technology

The University of Stavanger

The University of Stavanger

June 2016

Acknowledgements

Abstract

Low-frequency seismic analysis and direct hydrocarbon indicators

Bilal Ahmed Bhatti, M.Sc.

The University of Stavanger, 2016

Supervisor: R. James Brown; Børge Rosland

Low-frequency seismic analysis has been used as a possible direct indicator of the presence of hydrocarbons in reservoirs. Laboratory examples, synthetic studies and field examples in oil and gas exploration suggest that hydrocarbons often contribute a low-frequency anomaly (less than 15 Hz). There are a number of algorithms available in interpretation software packages that perform spectral decomposition of reflection seismic arrivals. Using seismic and well data from the Johan Sverdrup field, central North Sea, and the Western Graben, southern North Sea, a low-frequency analysis has been carried out in the context of differences in lithological properties of reservoirs. Spectral decomposition is applied to stacked seismic traces to enable low-frequency analysis and comparison of results from these two oil-bearing reservoirs types. To look for low-frequency anomalies, spectral sections of 5 Hz to 40 Hz have been used. Additionally, in order to analyze anomalous low-frequency responses, so-called frequency gathers (amplitude vs time in various narrow frequency bands) at a single seismic trace or well location have been used. This study focuses on finding a connection between the occurrence or non-occurrence of low-frequency anomalies and the nature – heterogeneous or homogeneous – of the reservoir. Here, Johan Sverdrup is considered a relatively homogeneous reservoir while the 2/7-31 discovery in Western Graben is considered a relatively heterogeneous reservoir.

TABLE OF CONTENTS

List of Tables

List of Figures

x

1 INTRODUCTION

Accumulating evidence suggests that hydrocarbons often exhibit a low-frequency anomaly (less than 20 Hz) in seismic data. Taner et al. (1979) observed anomalously high-amplitude low-frequency events associated with a gas reservoir. Since then, several studies, including: laboratory studies (physical modeling), synthetic studies (numerical modeling), and field examples have been reported in the literature, in which low-frequency anomalies indicate the presence of hydrocarbons. Physical modeling studies have been carried out by e.g. Goloshubin et al. (2002), Batzle et al. (2006), Madonna et al. (2010) and Nakagawa et al. (2016). Numerical modeling studies have been published by e.g. Castagna et al. (2003), Carcione et al. (2010), Silin and and Goloshubin (2010), Chen et al. (2012), Lefeuve-Mesgouez et al. (2012) and Huang et al. (2015). Several authors have observed low-frequency anomalies associated with hydrocarbon reservoirs in reflection-seismic exploration data, e.g. Goloshubin et al. (2002), Castagna et al. (2003), Goloshubin et al. (2006), Chen et al. (2012) and Zhong (2014). The mechanism responsible for these effects is still not clearly understood. However, several investigators have attempted to find out the possible cause of these effects.

Tai et al., (2009) described that when a seismic wave travels through the subsurface, the properties of the seismic wave – e.g. amplitude and frequency content – are affected by, among other things, geological structures, layer thicknesses, lithology, maturation of porosity and fluid properties in the reservoir. Then, when a wave reflects and return to a surface recorder, it brings back information about stratigraphic features, changes in rock properties and hydrocarbon presence. It is this information that we try to decipher based on our objectives. Tai et al. (2009) consider the phenomenon of low-frequency energy anomalies associated with reservoir zones (Figures 1 and 2). One sees in their analysis that the connection between hydrocarbon occurrence and the character of low-frequency anomalies is not always simple.

1
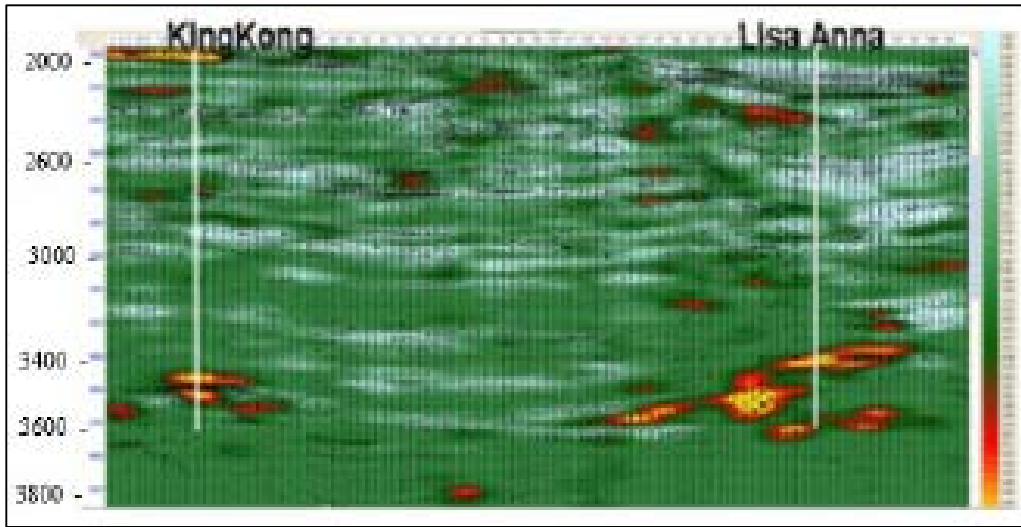
Figure 1: Modified from Tai et al. (2009): Low-frequency anomaly profile including two wells. CMPs and traveltime (ms) are plotted on the horizontal and vertical axes, respectively. The red-orange colors represent low-frequency anomalies.
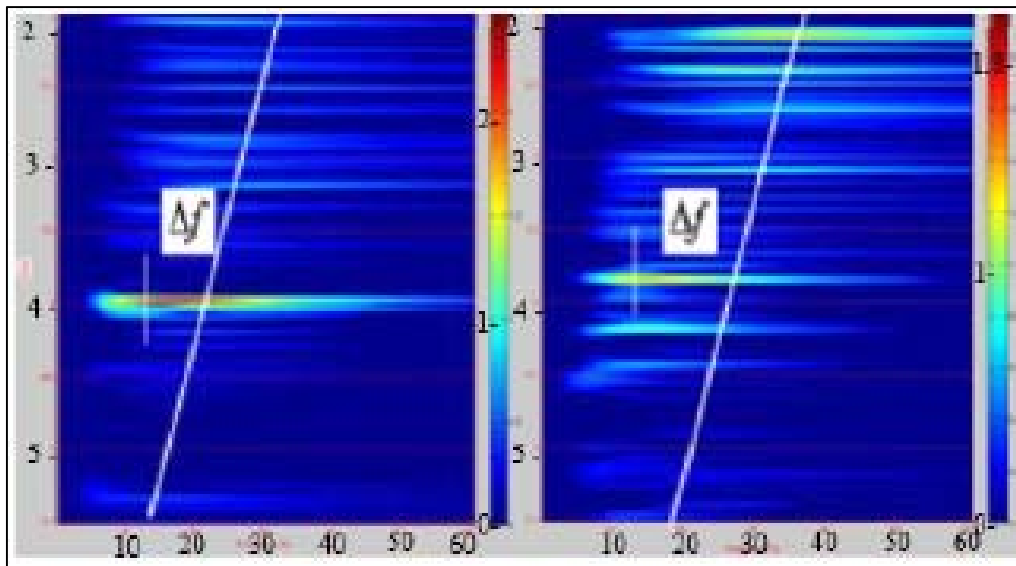
Figure 2: Frequency-versus-time sections of traces; frequency (Hz) (horizontal axis) against time (vertical axes) in seconds. Large shifts in the peak frequencies (red-orange colors) are at about 11 Hz and 14 Hz. The left-hand reservoir is commercial gas, the right-hand reservoir was dry (gas-fizz).

Extraction of the frequency components of seismic waves by spectral decomposition can be carried out by a number of algorithms. According to Castagna et al. (2003), spectral decomposition consists of three steps: "(1) decomposition of seismogram into constituent wavelets using wavelet transform methods; (2) summing up of the transformed spectra to produce 'frequency gathers'; and (3) sorting the frequency gathers to produce common (constant) frequency cubes, sections, time slices, and horizon slices. Finally, the results can be visualized by several animation techniques in interpretation software".

In terms of seismic reflection, spectral decomposition refers to any method or set of algorithms, also known as time-frequency distribution (TFD) techniques, that produce a continuous time-frequency analysis of a seismic trace (Lu and Li, 2013; Castagna and Sun, 2006). A number of TFD methods have been proposed for spectral decomposition in the literature and several commercial seismic processing packages include algorithms based on one of these: the short- time Fourier transform (STFT), continuous-wavelet transform (CWT), discrete Fourier transform (DFT), matching-pursuit decomposition and instantaneous spectral analysis (ISA) (Mallat and Zhang, 1993; Qian and Chen, 1994; Partyka et al., (1999); Castagna et al., 2003; Lu and Li, 2013). Each method has its own advantages and disadvantages, and different applications require different methods. Therefore, none of these methods, can be classified as 'right' or 'wrong'. However, the Gabor-Morlet transform, a subtype of CWT, often results in better resolution (Ahmad et al., 2016).

The short-time Fourier transform (STFT) converts the seismic signal to its frequency components and produces a 2D representative profile of frequencies versus time by adding a small time-domain window and shifting this window appropriately (Okaya et al., 1992; Zhong, 2014). This results in the vertical resolution to be fixed over the entire time-frequency plane.

The CWT is a commonly used wavelet transform that utilizes orthogonal basis wavelets in order to break down the seismic trace into individual frequency components. The CWT is essentially equivalent to a narrow-band filtering of the data in the temporal domain (Puryear and Castagna, 2008). In practice, the CWT has higher frequency resolution for low frequencies and better time resolution for higher frequencies (Chakraborty & Okaya, 1995). As an extensional version of CWT,

Stockwell et al. (1996) introduced an S-transform algorithm based on a moving and scalable localizing Gaussian window. Differentiating itself from other methods, the S-transform is an invertible transform that is closely related to the Fourier transform (Zhong, 2014).

The DFT consists of absolute use of windows, in such a way, that the nature of windowing has an enlightening effect on the spectral and temporal resolution of the output. Commonly, the DFT is used to evaluate the spectral components of long windows having several reflection events (Castagna and Sun, 2006).

The matching pursuit decomposition (MPD) was introduced by Mallat and Zhang (1993) to detect presence of low-frequency shadows below the hydrocarbon-filled reservoirs. The basic principle of MPD is that it involves the cross-correlation of a wavelet dictionary against the seismic trace. The best projected wavelet on a seismic trace is subtracted from that trace. The cross-correlation continues with the residual again, and the process of subtraction is repeated until the energy left in the residual falls below some suitable threshold. This process results in a series of wavelets along with their respective arrival times and amplitudes for each seismic trace. The wavelet series can be immediately converted to a time-frequency analysis by superposition of the wavelet frequency spectra (Castagna and Sun, 2006).

Castagna et al. (2003) presented a method known as instantaneous spectral analysis (ISA). The ISA is a continuous time-frequency analysis technique that decomposes each time sample of seismic trace to its frequency spectrum. As a result, a representation of amplitudes at different frequencies through time is acquired, also known as frequency gathers. This method avoids windowing problems that complicate conventional Fourier analysis and, hence, provides excellent resolution in terms of time and frequency localization (Figure 3).
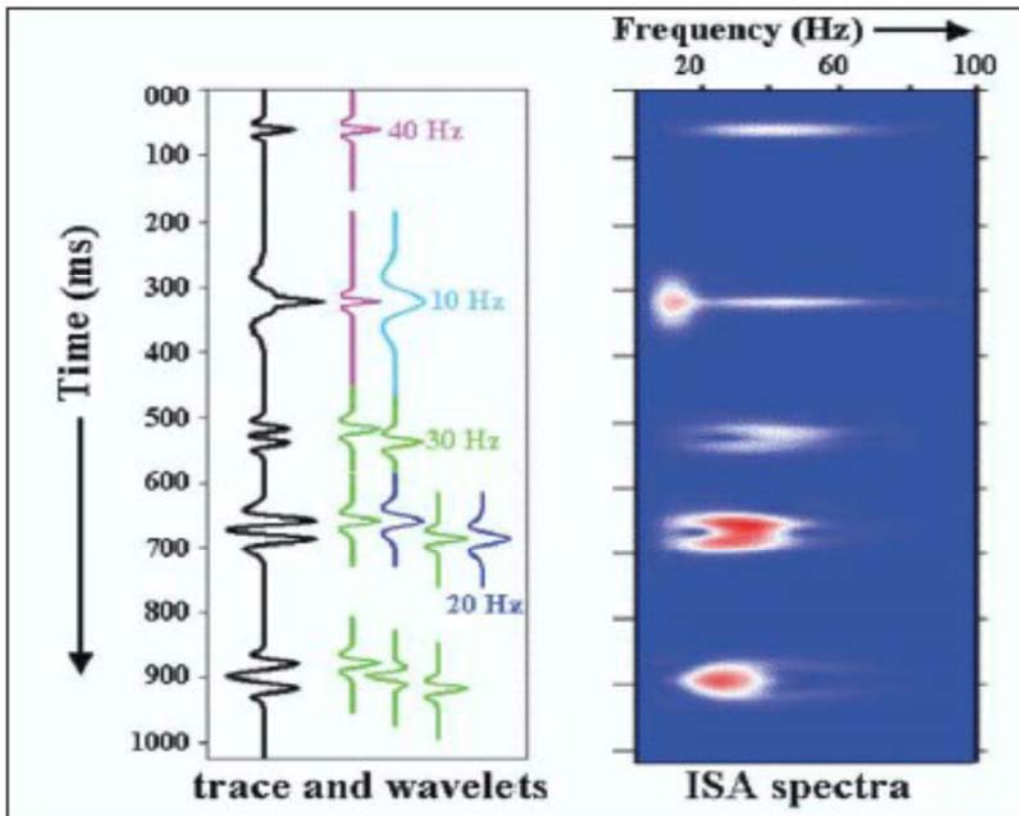
Figure 3: Synthetic waveform with transient arrivals (black seismogram), constituent wavelets (color coded by center frequency), and time-frequency analysis (red represents high amplitude).

Figure 4 is a low-frequency anomaly profile of Ay-Pim oild field, Western Siberia. It is observed that there are low-frequency anomalies present associated with oil-bearing zones (Goloshubin et al., 2002).
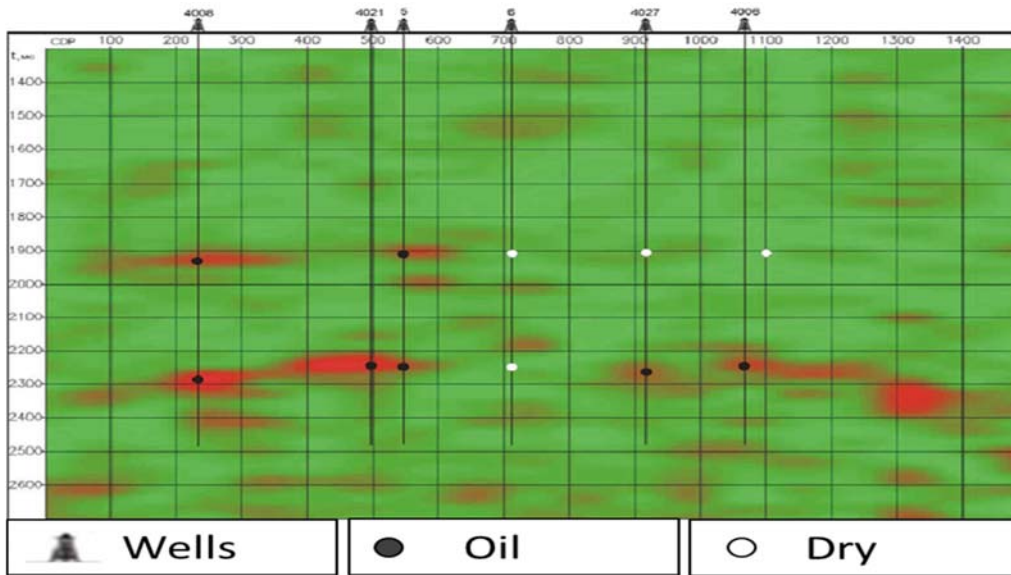
Figure 4: Modified from Goloshubin et al. (2002): Low-frequency anomaly profile of Ay-Pim oil field, Western Siberia, including six wells . CMPs and traveltime (ms) are plotted on the horizontal and vertical axes, respectively. The red-orange colors represent oil-bearing low-frequency anomalies.

Asymptotic numerical analysis of Biot's theory of poroelasticity by Goloshubin and Chabyshova (2012) exhibited converted fast-slow-fast P-waves (Figure 5) from a thinly layered porous permeable fluid-saturated model of a sandstone reservoir and the seismic frequency response. According to their hypothesis, any low-frequency anomaly is expected to be weakest in massive homogeneous thick reservoirs and strongest for highly interbedded permeable reservoirs. Therefore, gas shadows can potentially indicate not only hydrocarbons but reservoir quality as well.
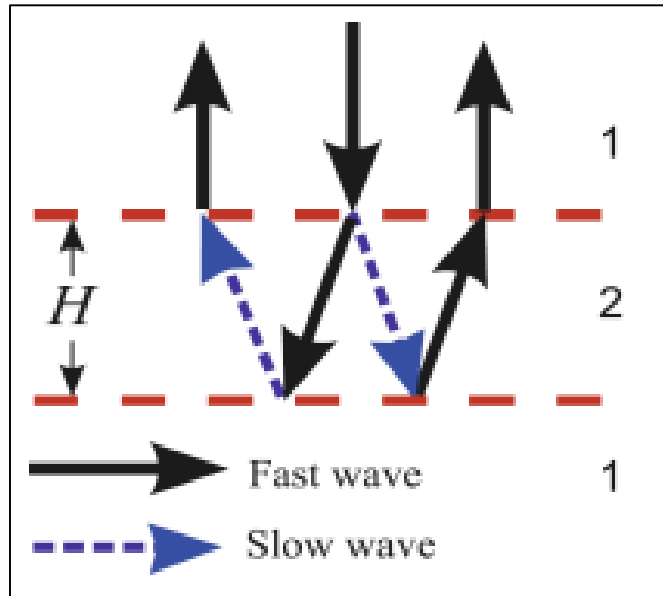
Figure 5: Pattern of P-wave reflections from thin permeable layer (layer 2) based on converted fast-slow-fast waves (Silin and Goloshubin, 2010)

The objective of this study is to test their hypothesis by comparing the low-frequency response of the relatively homogeneous massive sandstone reservoir of the Draupne Fm (Johan Sverdrup field, Central North Sea) with the relatively heterogeneous permeable reservoir containing silty sand of the Ula Fm, Eldfisk Fm and Tor Fm (Western Graben, Southern North Sea). Therefore, the emphasis will be finding a connection between the occurrence or non-occurrence of low-frequency anomalies and the nature – heterogeneous or homogeneous – of the reservoir.

To provide a detailed reservoir analysis, lithofacies classification is performed by generating V_P-porosity plots in Petrel 2015 to identify fine sand, sand and shale. These plots result in classifying types of reservoirs based on their relative homogeneity and heterogeneity.

In oil and gas exploration, several types of logging techniques, such as core-logging, petrophysical logging, geophysical logging, etc., have been widely used. They are highly effective due to their direct measurement (Fanka, 2012). Hossain and MacGregor (2014) proposed a new method, called the rock physics diagnostic (RPD), which is widely used to understand the functional relationship between seismic

velocities and porosity. The idea of this analysis is to classify lithology within a specific zone by quantifying the amount of contact and pore-filling cement. Thus, classification into clean-sand, shaly-sand or shale can be done by using RPD.

There are a number of rock physics models presented in the literature and several available interpretation software packages to investigate fluid and lithology. Some of them are used in this project and inserted into V_P-porosity plots for lithofacies classifications. These models include provision for contact-cement, constant-cement and friable-sand models, representing the clean-sand, shaly-sand and shale classifications, respectively.

The contact-cement model explains variation of velocity with porosity with respect to cement volume at high porosities (Fanka, 2012). Moreover, that model describes the excellent sorting of sandstones, whereas, in constant-cement cases, more poorly sorted sandstones are modeled (Avseth et al., 2010). The friable sand model was introduced by Dvorkin and Nur (1996). It takes into account the changes in velocity-porosity relationship with poor sorting of sandstones. They assumed that porosity decreases as compared to the initial critical porosity value due to the deposition of the solid matter away from the grain contacts. Hence, this model is a representation of less sorted and less cemented sandstones (Figure 6).
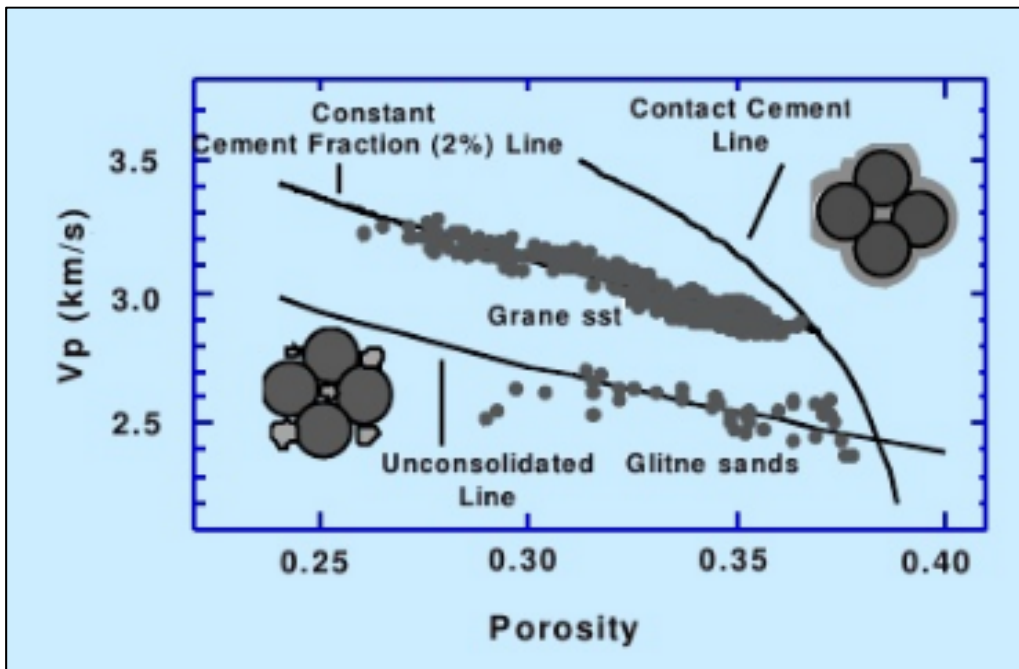
Figure 6: Modified from Avseth (2012). A plot of V_P versus porosity showing 3 models: contact-cement, constant-cement and unconsolidated-line (friable-sand). As V_P and porosity increase, the sorting changes from poor to good.

2 DATA AND METHODOLOGY

The database for this study comprises well data from 22 wells and two post-stack full-offset migrated 3D broadband seismic datasets: CGG-R14 located in Johan Sverdrup field, central North Sea (Figure 7) and MC3D-CGR2012 located in the Western Graben, Southern North Sea (Figure 8). Both datasets are displayed in negative polarity as indicated by SEG polarity convention for zero-phase display. Thus, a downward increase in acoustic impedance is represented by a central zero-phase trough, and vice versa. Well logs provided for this study include gamma-ray, caliper, neutron porosity, density, resistivity, sonic logs etc. Frequency cubes of 5 to 40 Hz were also gathered by spectral decomposition of seismic cubes in IHS Kingdom software.
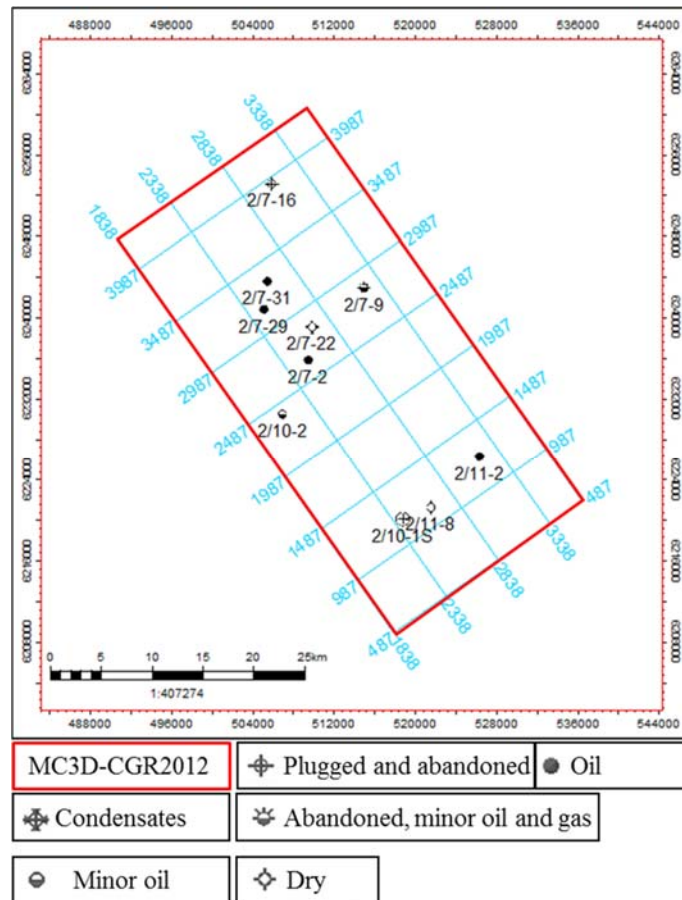
Figure 7: MC3D-CGR2012 seismic cube acquired in southern North Sea.
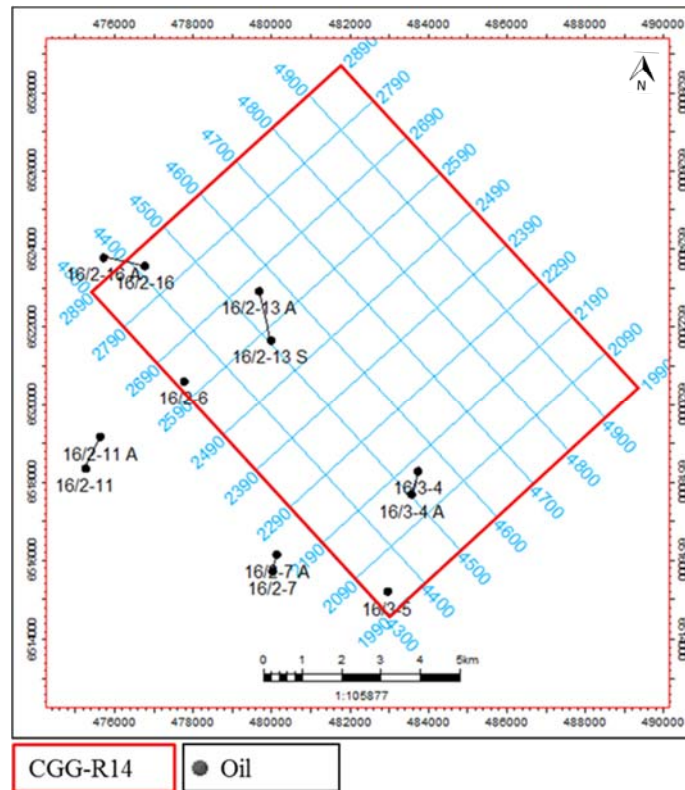
Figure 8: CGG-R14 seismic cube acquired in central
North Sea (Johan Sverdrup field).

To determine the vertical resolution of seismic data, IHS Kingdom's 'tuning analysis' was performed on both of the seismic cubes used for this study (i.e. MC3D-CGR2012 and CGG-R14. According to the results, the minimum separable time-thickness for MC3D-CGR2012 is 22 ms and that for CGG-R14 is 18 ms (Figures 9 and 10).
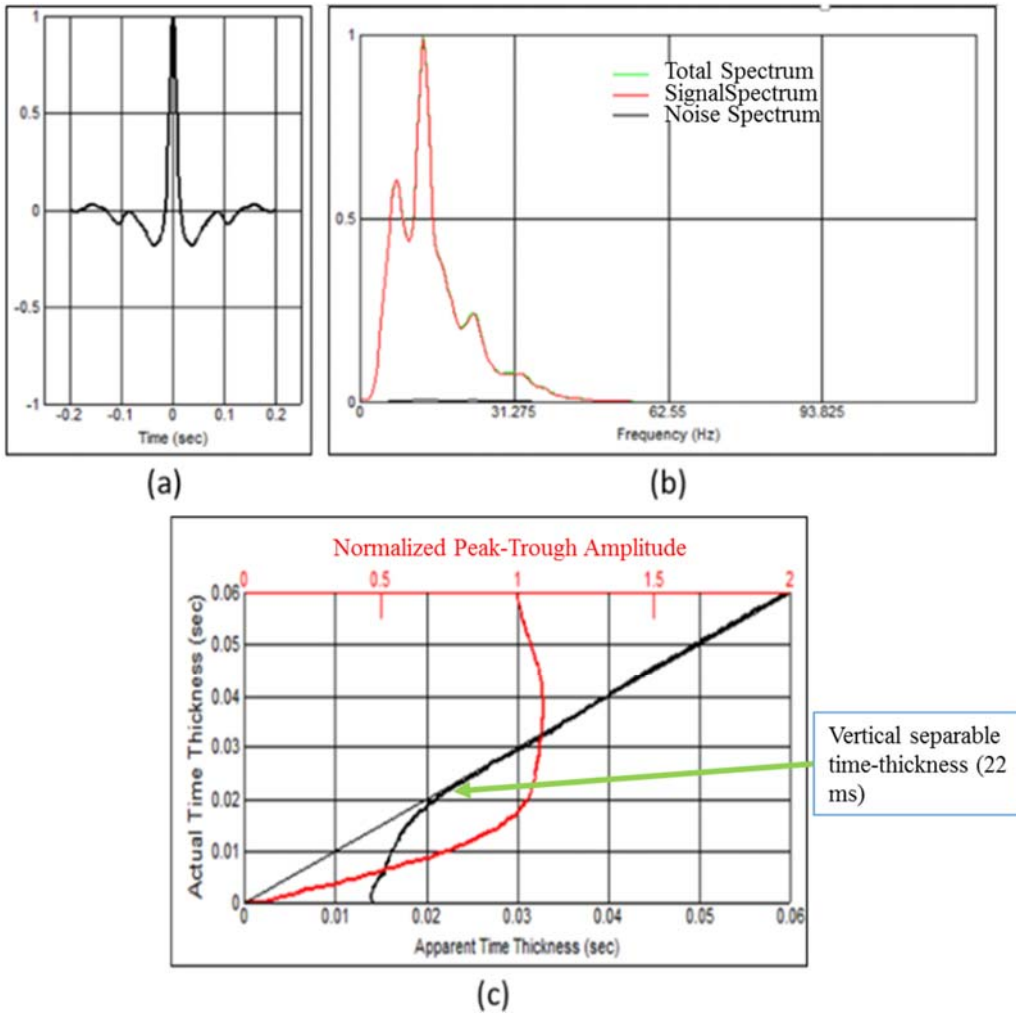
Figure 9: PSTM gather computation for MC3D-CGR2012: a) computed wavelet; b) computed spectrum; c) tuning thickness analysis.
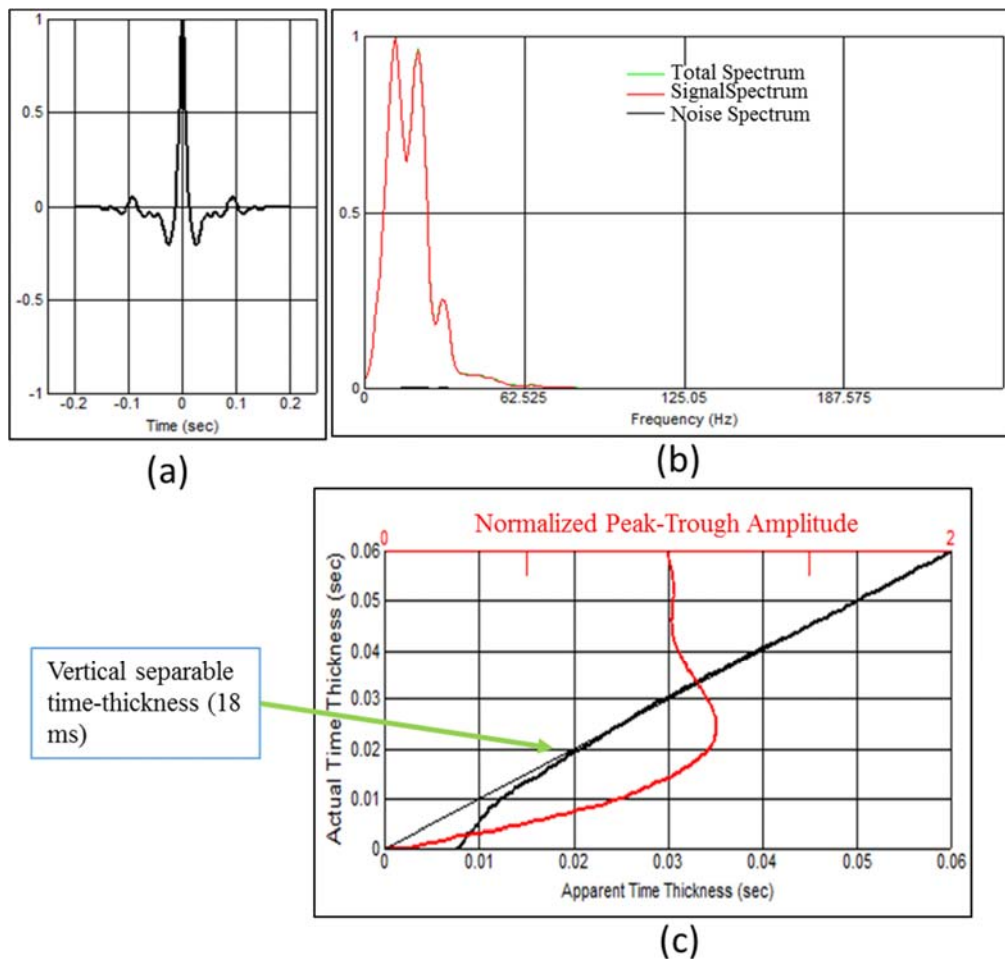
Figure 10: PSTM gather computation for CGG-R14: a) computed wavelet; b)
computed spectrum; c) tuning thickness analysis.

After loading the well and seismic data into the interpretation software, well-log analysis and lithofacies classification using rock physics were carried out to differentiate between the lithological properties of the two reservoirs. This was done by creating rock physics models (contact-cement, constant-cement and friable-sand) under 'Rock Physics Toolbox' provided by Cegal, in Petrel 2015. After generating these models, several steps were considered before superimposing them onto V_P versus porosity plots.

To tie the well to the seismic data, synthetic seismograms were generated. Itnitially to do so, sonic calibration was done, followed by generation of several

wavelets and synthetic seismograms. The best results obtained were by using deterministic method and extended white algorithm for generating wavelets. However, several methods were used in trying to match the synthetic data with the seismic data.

After performing seismic-to-well ties, several horizons were picked in both stacked migrated 3D datasets. In CGG-R14, the Draupne Fm of the Upper Jurassic and Ekofisk Fms were picked. And in MC3D-CGR2012, the Basal Cretaceous Unconformity (BCU) and the Ula Fm of the Late Jurassic were picked in time.

Finally, spectral decomposition was performed to analyze the low-frequency responses of the two different reservoirs. For this purpose, spectral sections of constant frequencies were acquired in IHS Kingdom software, which uses 'Rock Solid Attributes' to carry out spectral decomposition. Additionally, ISA gathers (frequency versus time plots) were also generated in OpendTect 6.0 to analyze the frequency response through time on a single trace.

3 GEOLOGICAL SETTING

Sørlie et al. (2012) describe the Johan Sverdrup discovery, made in August 2010 in well 16/2-6, PL 501, located in the central North Sea (Figure 12). It is described as "a fault-bounded trap against the Southern Utsira Basement High and overlying Jurassic shales and/or Cretaceous Åsgard marls. The main reservoirs consist of a sequence of Middle and Upper Jurassic sandstones of excellent quality. The Volgian age sandstones of the Draupne Fm, consist of unconsolidated, massive homogeneous sands and are thought to represent an amalgamated marine, high-density gravity flow or bedload deposits". Geologically, the Utsira high is located west of Patch Bank Ridge, north of Ling depression and east of the Gudrun terrace.

MC3D-CGR2012 is located in the Western Graben, located in the southern North Sea, approximately 260 km SW of Farsund on the southwest coast of Norway, and is adjacent to the United Kingdom and Denmark sectors (Figure 13). Geologically, this area is located between the Lindesnes Ridge to the northeast and the Grensen Nose to the southwest. This area has proven hydrocarbon potential and several oil and gas fields have been discovered on Lindesnes Ridge, e.g. Eldfisk, Embla and Vallhall, among others, from Jurassic and Cretaceous reservoirs (Gennaro et al., 2013). The main reservoirs reported in the literature are: carbonates of Late Cretaceous at Valhall, fluvial sandstones of Devonian to Permian age in the Embla field, and chalks of Paleocene in the Eldfisk.
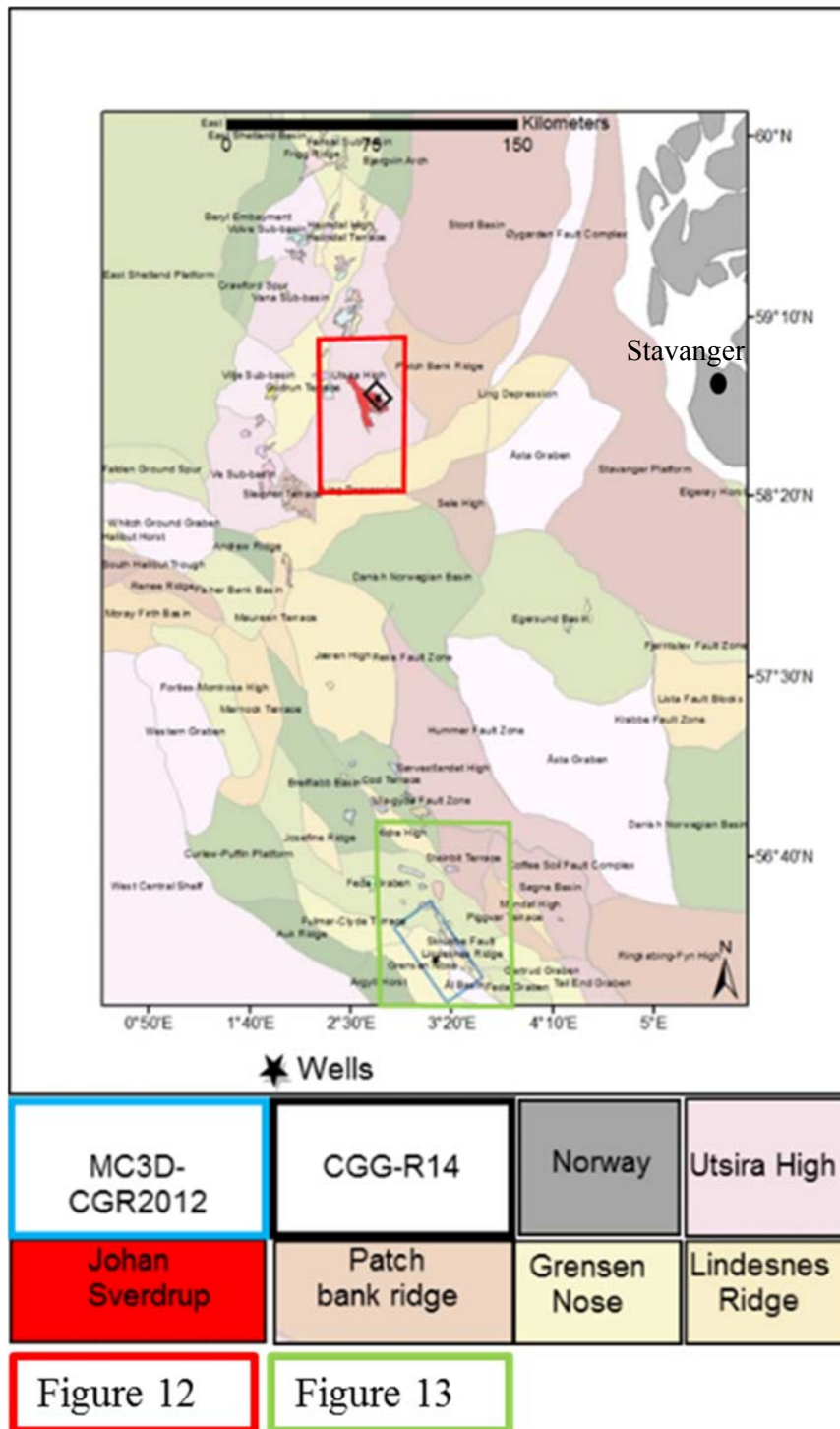
Figure 11: Location map of study areas.
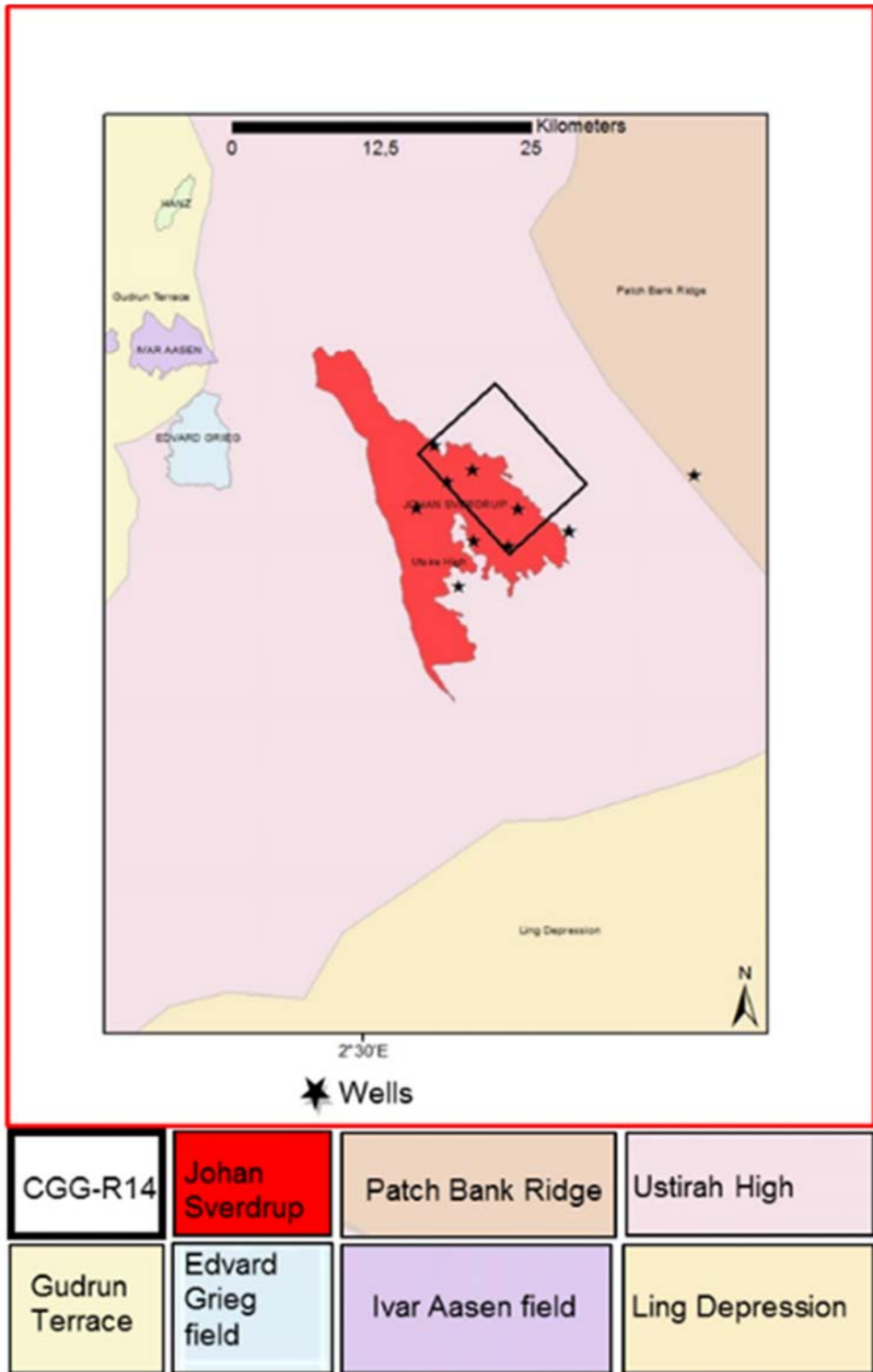
Figure 12: Location of study area in Johan Sverdrup field, central North Sea.

17
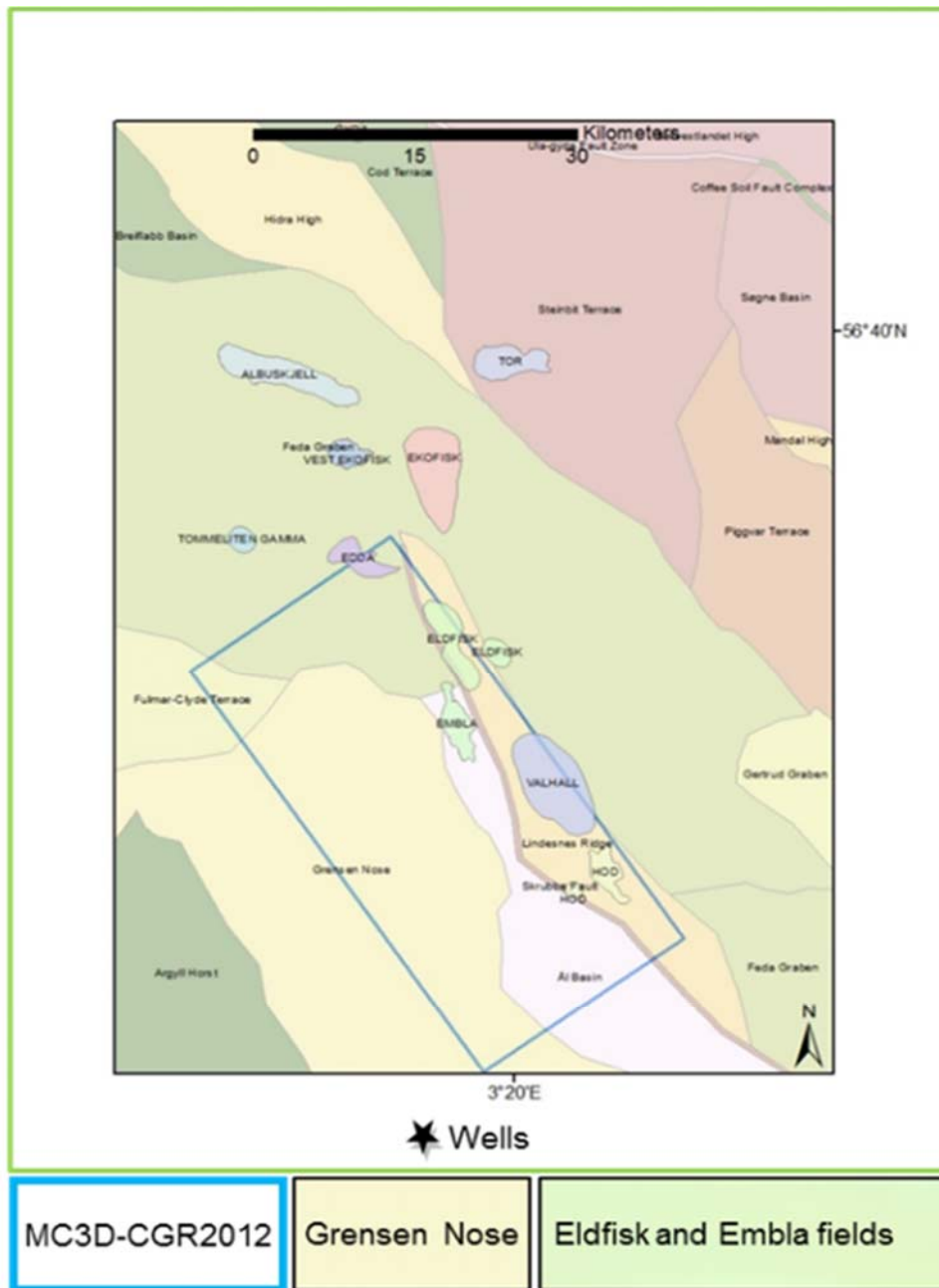
Figure 13: Location of study area in Western Graben, southern North Sea.

3.1 Tectonic History

Jackson et al. (2010) gave an account of the structural evolution in the Utsira high through time. A series of minibasins formed on the southwest margin of the Utsira high during the Triassic to early Middle Jurassic due to the mobilization of the salt-rich Zechstein Supergroup (Upper Permian). During the Middle-Late Jurassic, the overburden caused a collapse of the underlying salt bodies and a series of secondary minibasins started to develop. The development of minibasins during the Triassic and Jurassic influenced the routing of submarine sediment gravity flows (the Draupne Fm) and fluvial channel systems (Skagerrak and Sleipner Fms) (Figure 14).

The southern part of the North Sea experienced several tectonic stages: (1) the first extension and rifting episode from Carboniferous to Permian; (2) second extension and rifting episode during Triassic; (3) third extension and rifting episode during middle to late Jurassic; (4) end-Jurassic compression; (5) fourth rifting episode and onset of sea-floor spreading during early Cretaceous; and (6) onset of sea-floor spreading and renewed rifting from late Cretaceous to early Paleogene (Figure 15) (Müller et al., 1992; Brekke, 2000; Mosar, 2003; Wilson et al., 2006; Gołedowski et al., 2012; Rossland et al., 2013; and Zhong, 2014).
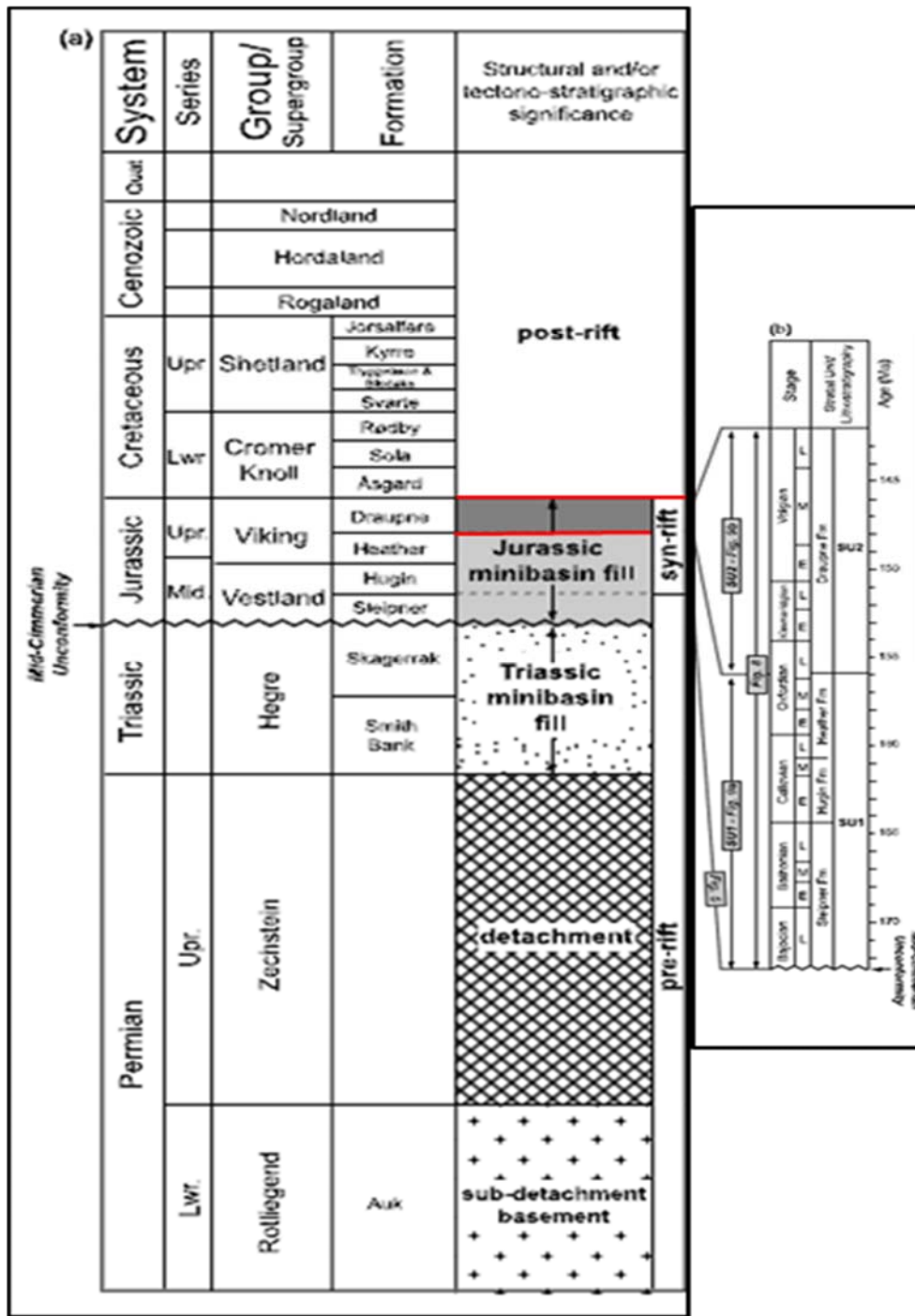
Figure 14: Modified from Jackson et al. (2010): a) Composite stratigraphic column for the Norwegian sector of the northern part of the SVG; b) Detailed stratigraphic column focused on the Middle to Upper Jurassic, late pre-rift to syn-rift interval of interest.
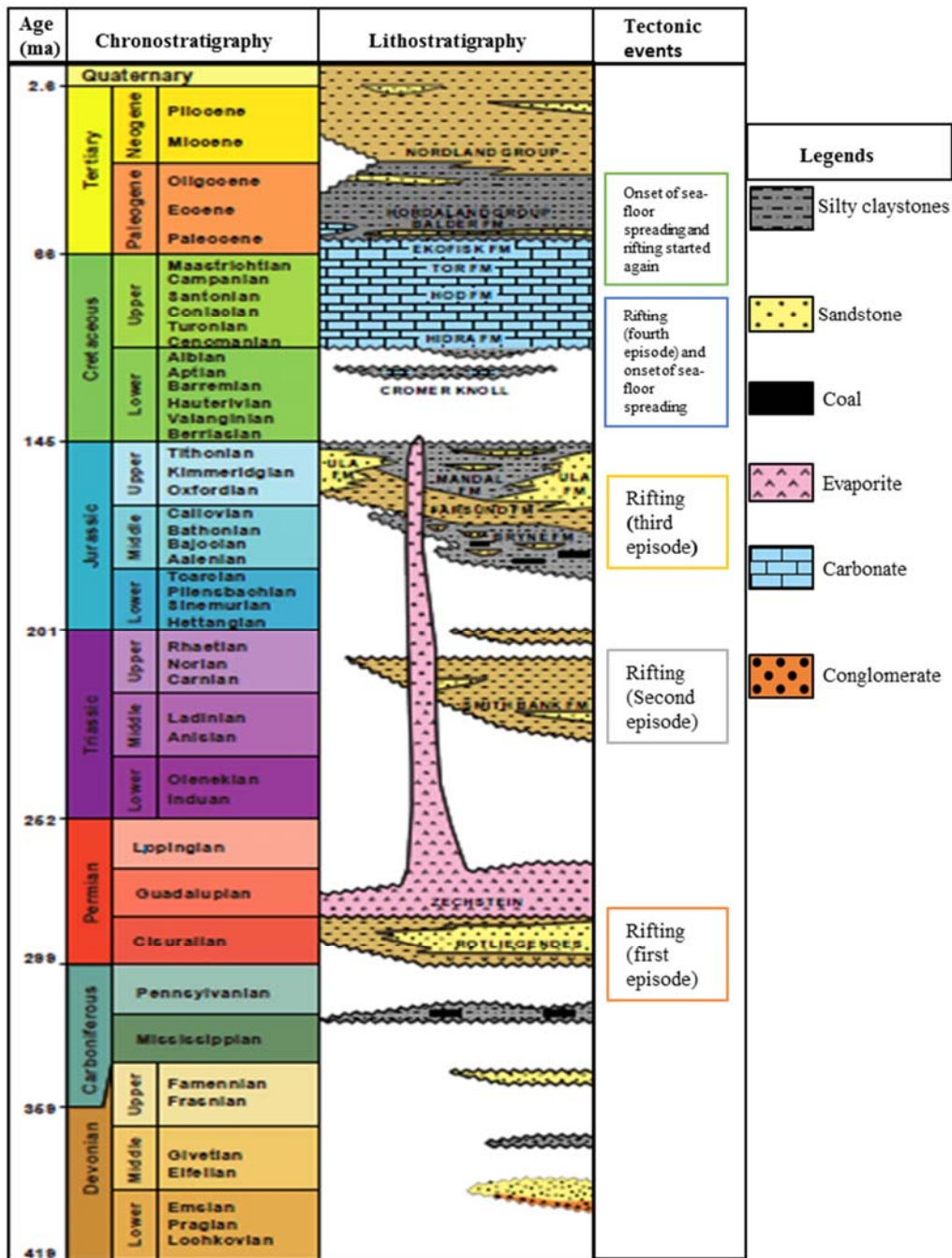
Figure 15: Stratigraphic chart of southern North Sea (Deegan et al., 1977; Casey et al., 1993; Lee et al., 1993; Blystad et al., 1995; Brasher et al., 2013; Rossland et al., 2013; Zhong, 2014).

3.2 Hydrocarbon discoveries

Most of the wells that have been drilled in both the study areas encountered hydrocarbons (NPD, 2016). There are a number of producing fields surrounding both the study areas, for example, Edvard Grieg and Ivar Aasen fields (northwest of Johan Sverdrup filed, Figure 12), Eldfisk and Embla fields (located on Lindesnes Ridge, Figure 13).

3.2.1 Central North Sea

3.2.1.1 EDVARD GRIEG

Edvard Grieg is an oil field located in the Utsira High area in the central North Sea. The reservoir contains undersaturated oil in the Upper Triassic to Lower Cretaceous alluvial, eolian and shallow marine conglomerates and sandstones. There are proven oil reserves in the underlying basement. There is a 40 m thick reservoir present from 1900 to 1940 m depth (NPD, 2016).

3.2.1.2 IVAR AASEN

The Ivar Aasen oil field was discovered by the Norwegian oil company Det Norske in 2009. It is located west of the Johan Sverdrup field in the North Sea and contains around 200 million barrels of oil equivalent. Well 16/1-9 drilled in Ivar Aasen shows that the reservoir consists of shallow marine sand in the Hugin Fm and fluvial sand in the Sleipner and Skagerrak Fms of Middle Jurassic to Late Triassic age. The reservoir contains oil at a depth of about 2400 m. Parts of the reservoir have an overlying gas cap (NPD, 2016).

3.2.2 Southern North Sea

3.2.2.1 ELDFISK

Eldfisk is an oil field located in the southern part of the Norwegian sector in the North Sea. Geologically, it is located in the northern part of Lindesnes Ridge. The Eldfisk field produces from chalk in the Ekofisk having four-way dip closure. Significant anticlines were generated due to salt diaprism from the Upper Permian Zechstein group penetrated through overlying beds. The reservoir rock has high

porosity with low permeability. Natural fracturing allows the reservoir fluids to flow more easily (Jenyon 1985; Herrington et al., 1991; NPD, 2016).

3.2.2.2 EMBLA

Embla is an oil field with high pressure and high temperature (HPHT) near Eldfisk in the southern part of the Norwegian sector of the North Sea. Geologically, the Embla field is located on the western flank of Lindesnes ridge. It was discovered in 1974 by the 2/7-9 well, and it has structural and stratigraphic traps with shales sealing on top. The reservoir in Embla consists of segmented sandstone and conglomerate reservoir of Devonian and Permian age. The reservoir is complex and is located more than 4000 meters deep (Ahmadi et al., 2003; NPD, 2016).

3.3 Well analysis

A brief review was performed on the key wells in both the study areas to know the content, objectives and reservoir details about the wells. All the information about wells is taken from the Norwegian Petroleum Directorate (NPD, 2016).

3.3.1 Central North Sea

16/2-16 (Oil)

The main objective was to acquire information about the Jurassic reservoir properties and hydrocarbon column in this part of the field.

In total 15 m of net sandstone was found within a 60 m Jurassic sequence. The top of the reservoir was penetrated at 1950 m as prognosed. The oil/water contact was identified at 1952 m just above the good reservoir sand. The total depth of well was 2214 m (NPD, 2016).

16/2-13 S (Oil)

The main objective was to confirm an oil saturated Upper Jurassic Draupne sand thickness of approximately 30 m in the northeastern part of Johan Sverdrup.

The Draupne Fm shale was encountered at 1914.5 m and Intra Draupne Fm sandstone was drilled from 1924.4 m to 1939.9 m. A 25 m oil column was confirmed in these sandstones. The well was penetrated to a total depth of 2090 m (NPD, 2016).

16/3-5 (Oil)

The main objective was to determine presence and thickness of the Late Jurassic intra-Draupne Fm sandstone in a representative part of the Avaldsnes high (informal basement structure).

The well encountered top Draupne fm shales at 1909 m and the Intra-Draupne Fm sandstone at 1918 m. An oil column of approximately 30 meters was found in the Intra Draupne sandstone and Permian carbonate. The well proves an excellent development of the Late Jurassic sandstone in the southern part of the Avaldsnes High. 16/3-5 was penetrated to a total depth of 2050 m (NPD, 2016).

3.3.2 Southern North Sea

2/7-2 (Oil)

Well 2/7-2 was drilled on the Grensen in the Central Graben of the North Sea. The primary targets of drilling were to test the presence of Paleocene Sands and Danian Limestones; the secondary targets were Late Cretaceous carbonates, Early Cretaceous sandstones, Jurassic sandstones, and possibly Permo-Triassic sandstone reservoirs.

The Tor Fm was encountered at 3005 m depth and hydrocarbons were reported. Core samples were taken from 3013.9 to 3027.9 m (cores 1 and 2) which represented good oil shows. The well was penetrated to a total depth of 3964 m (NPD, 2016).

4 HOMOGENEITY AND HETEROGENEITY OF RESERVOIRS

Reservoir homogeneity and heterogeneity are concepts often used in scientific literature relating to the uniformity of reservoirs. A homogeneous reservoir may have uniform composition, or massive sand packages, whereas, reservoir heterogeneity refers to comparatively non-uniform reservoirs that may consist of thin sand-shale successions.

4.1 Critical well analysis

Analysis of the three wells has been carried out in this study: The 16/3-4 well is situated in Johan Sverdrup field, central North Sea. It was drilled to prove the extension of the Avaldsnes discovery to the northeast of the structural crest of the Avaldsnes structure. The Base Cretaceous Unconformity (BCU) was encountered at a depth of 1914 m. It included a 12 m thick package of shales on top of the 13.8 m thick Intra-Draupne Fm sandstones detected at 1926 m. The Intra-Draupne sandstone was oil-filled down to weathered basement at 1940 m. A DST was performed over Ula Fm sandstones in the interval 1923.5 to 1936.5 m. The test produced in the main flow 18,200 Sm^3 of gas and 885 Sm^3 of oil per day through a 52/64" choke (NPD, 2016). Figure 16 is the log response of well 16/3-4. The gamma-ray log shows a smooth trend in the reservoir having massive homogeneous sandstone with high porosity values and exceptionally high permeability. Resistivity values abruptly increase where the reservoir is hydrocarbon-saturated. Similar logs patterns were observed from other wells in the Johan Sverdrup field, e.g. 16/3-5, 16/2-16 and 16/2-13 S.
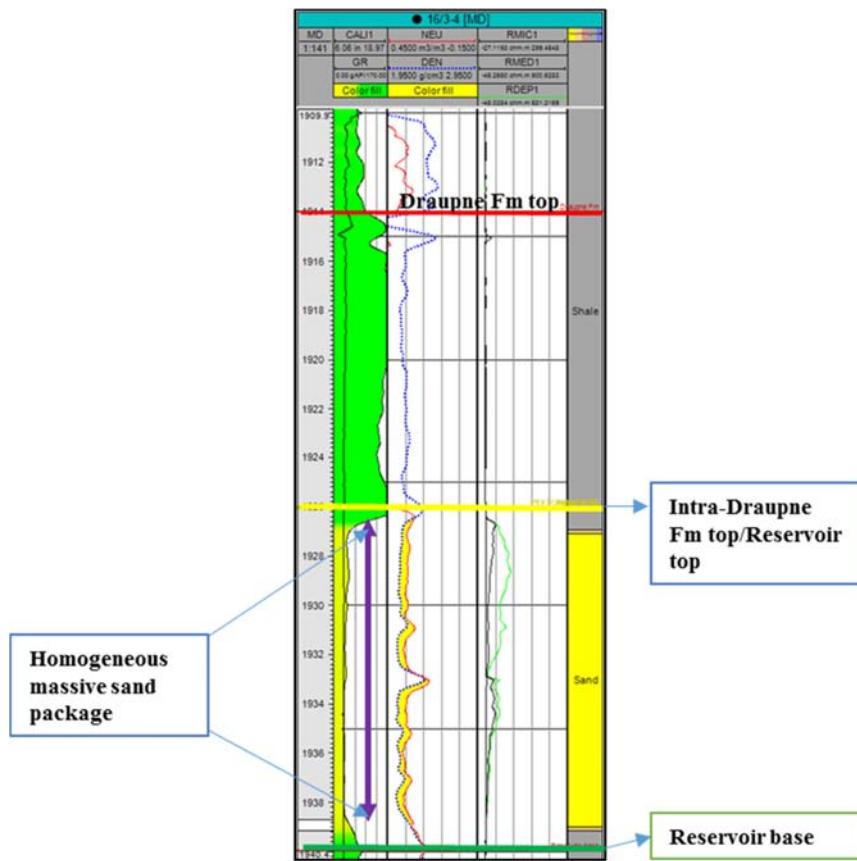
Figure 16: Well-log responses of well 16/3-4. The logs include: gamma-ray, neutron porosity and density (cross-plot) and resistivity log. Seismic data for 16/3-4 is taken from seismic cube CGG-R14.

The 2/7-31 well was drilled in the Western Graben to test the hydrocarbon potential of Upper Jurassic fluvial sand lenses of the Ula Fm. The well encountered hydrocarbons, first in the Lower Cretaceous Tuxen Fm (top 4372.1 m), then in the sandstones of the Lower Jurassic Ula Fm (4483.6 m) and finally in the Bryne Fm (top 4750 m). A DST over Ula Fm sandstones was performed in the interval 4565.9-4623.8 m. The well flowed at an average stabilized rate of 283 Sm^3 (NPD, 2016). From the gamma-ray log shown in Figure 17, the reservoir consists of mostly sandstone, but interbedded with thin layers of shale. Moreover, the reservoir is of higher impedance than the overlying shales.
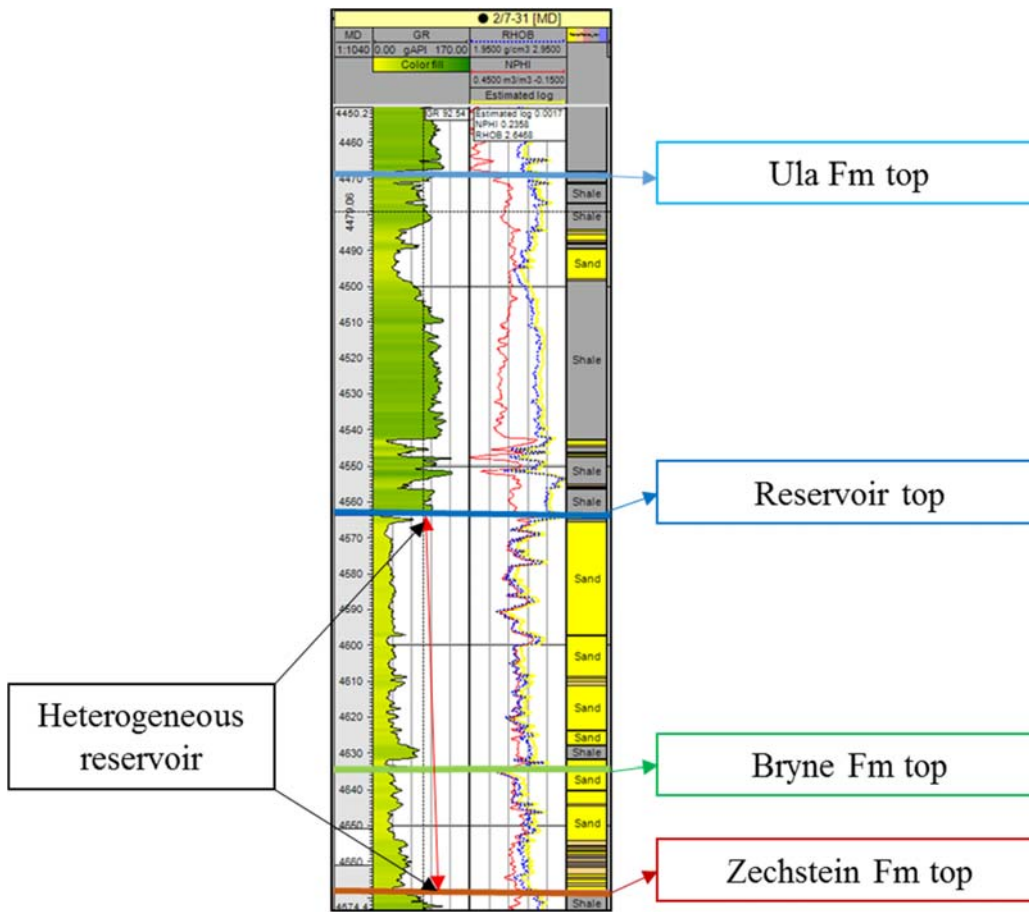
Figure 17: Well-log responses of well 2/7-31. The logs include: gamma-ray and neutron porosity and density (cross-plot). Seismic data for 2/7-31 is taken from seismic cube MC3D-CGR2012.

The well 2/7-29 was drilled to test the presence, quality and fluid content in Jurassic sandstones in prospects JU2 and JU7. Hydrocarbons were encountered in 49 m of net sandstone in the JU2 prospect (Eldfisk Fm). No drill-stem test was performed (NPD, 2016). The gamma-ray log response of the Eldfisk sandstone reservoir (Figure 18), showed a spiky behavior similar to that seen in the Ula Fm (well 2/7-31). There is a sharp ascent in resistivity values in the reservoir, starting from 4480 m down to 4530 m.
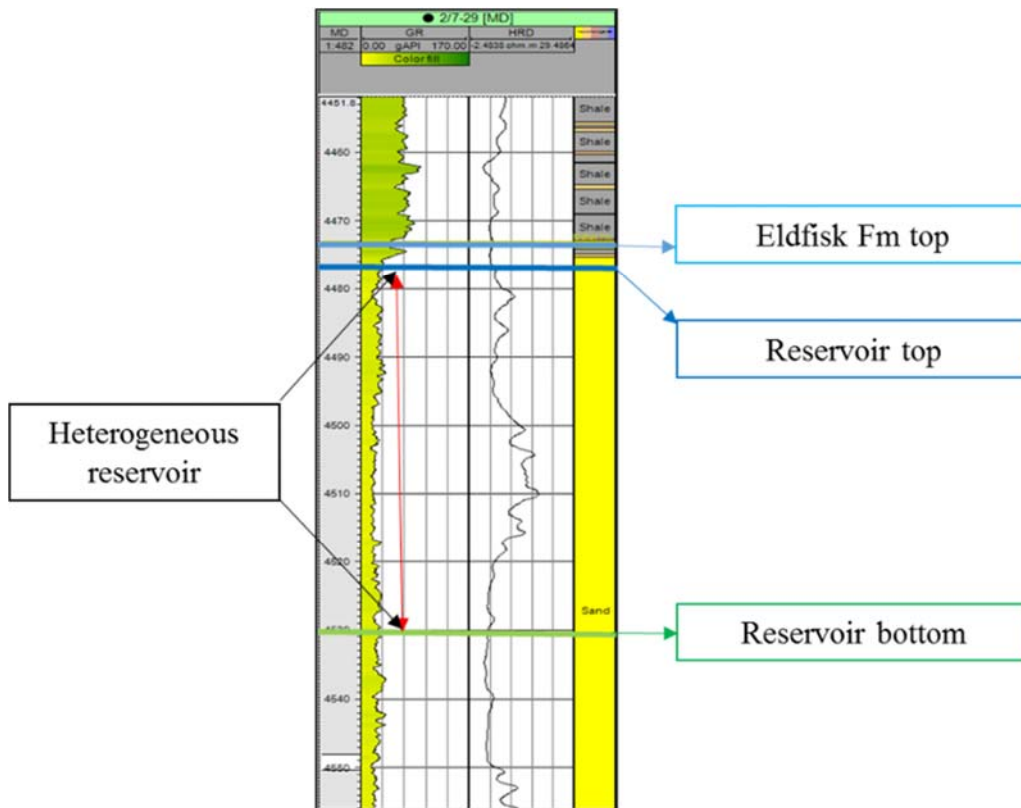
Figure 18: Well-log responses of well 2/7-29. The logs include: gamma-ray and resistivity log. Seismic data for 2/7-29 is taken from seismic cube MC3D-CGR2012.

In order to investigate further the lithological properties of the reservoir, several core photos were taken (NPD,2016). Figure 19 shows the coring samples from well 2/7-29 in the Eldfisk Fm in the depth interval 4483-4506 m. It consists predominantly of sandstone but contains considerable interbedded shales. The sandstone is dark yellowish brown to black (blackness could be due to hydrocarbons), fine- to coarse-grained, poorly sorted and angular. The Eldfisk Fm represents an influx of sand into the axial portions of the central Graben at a time of regression, consistent with a turbiditic origin of the formation (NPD, 2016).
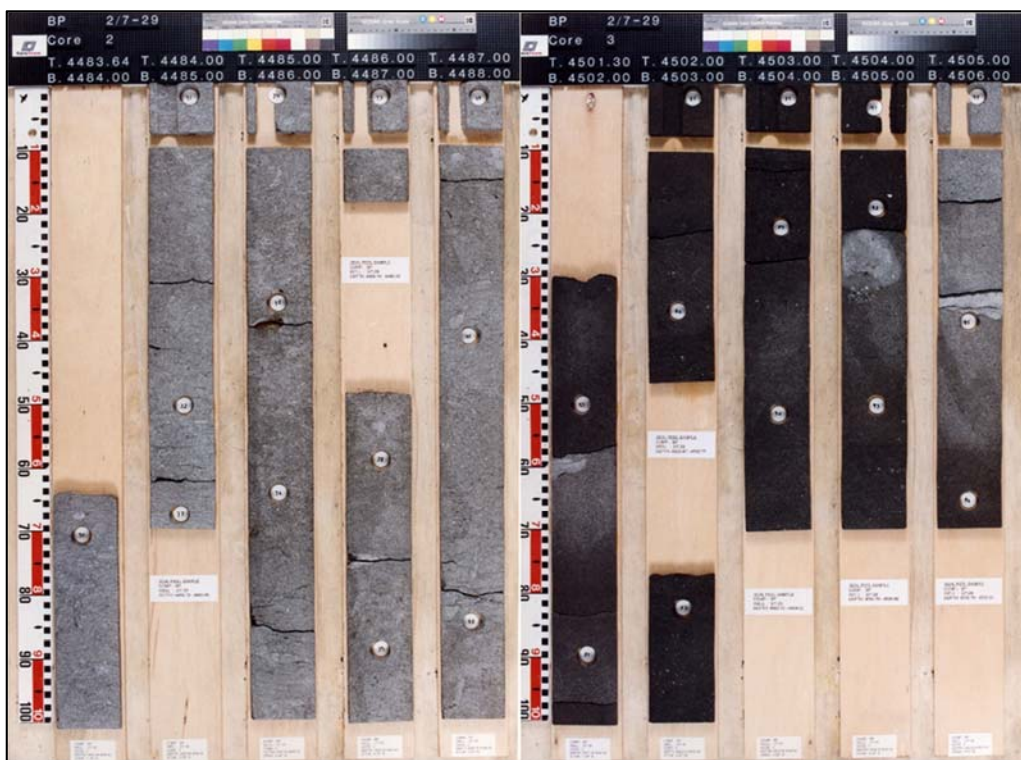
Figure 19: Photo of core sample in well 2/7-29. The depth interval is given from left to right, i.e, 4483.64 to 4506 m.

4.2 Rock physics

The high accuracy of direct log measurements makes its use highly applicable. To identify the lithology in the wells, several facies were generated in Petrel 2015 (using Blueback plugins) based on gammay-ray log values. These facies were generated by gamma-ray log values, including: sand (<60), fine sand (>50 and <60) and shale (>60) as shown in Figure 20.
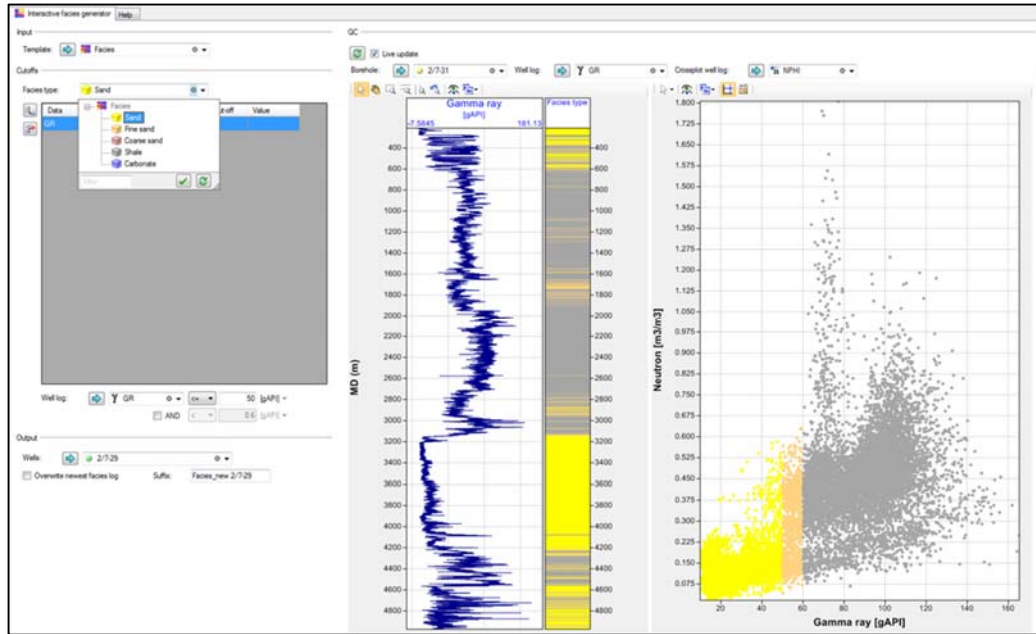
Figure 20: Facies generation by gamma-ray log.

To understand and distinguish the lithological properties of the two reservoirs in detail, V_P-vs-porosity plots were made in Petrel 2015. The classification is done based on three models: contact-cement, constant-cement and friable-sand.

The log response of well 16/-3-4 (Figure 16) shows that the reservoir is composed of homogeneous thick sandstone. Similar response is observed in V_P-vs-porosity plot (Figure 21), in which all the data plotted are taken only from the reservoir interval. It is observed that, these sandstones have very high porosity values and most of the points are located near to the contact-cement line. This could be a result of the

31

good sorting of grains (homogeneity) in the reservoir, which includes a thick sand package with cement coating which is helpful in preserving the resultant higher porosity.
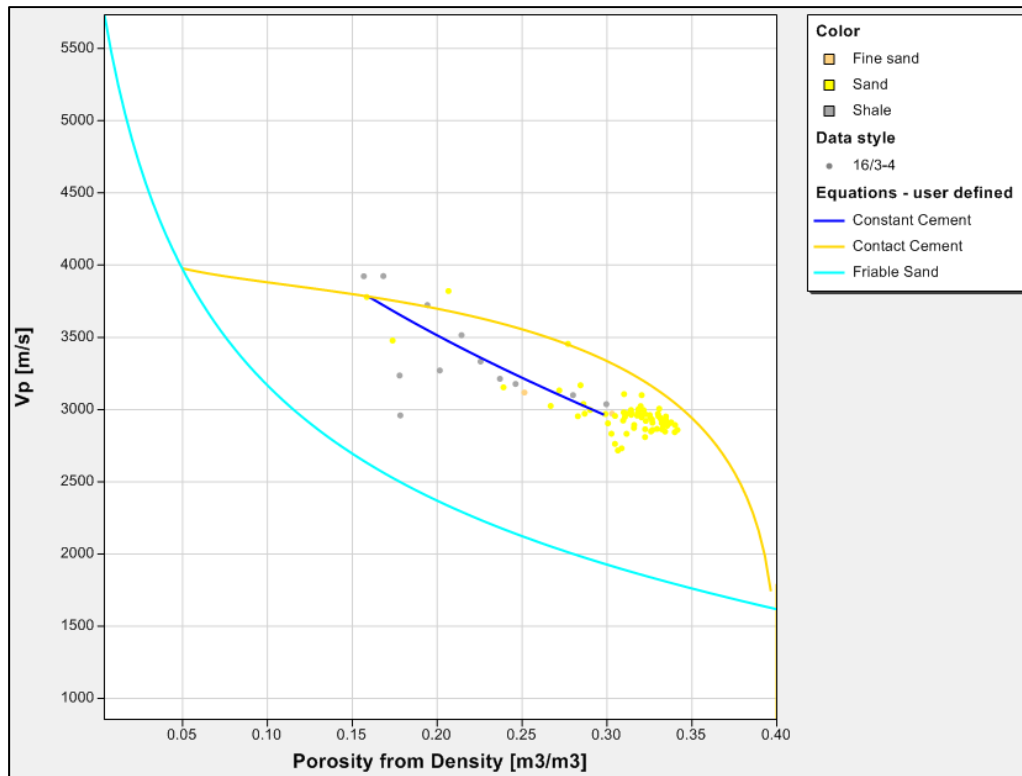
Figure 21: V_P-porosity plot of well 16/3-4 in the reservoir interval. Yellow, blue and turquoise-colored lines represent the contact cement, constant cement and friable sand models, respectively.

On the other hand, in the Ula Fm interval of well 2/7-31, a so-called heterogeneous reservoir can be inferred by observing the log response (Figure 17). This leads one to expect a similar response in lithological classification plots as well. In Figure 22, it is observed that oppositely to the reservoir of Draupne Fm, in Ula Fm reservoir, the majority of the scattered points lie on the constant-cement model. This means that the reservoir consists of sandstone with comparatively little compacted and poorly sorted sandstone. Nonetheless, there are some points that are plotted along the

friable-sand model representing sandstones without any cementation. These points may represent the presence of silty sand content that is interbedded in the sandstone.

Additionally, some evidence for the compaction trends was also seen by making plots of V_P-vs-depth. It is observed from these plots in Figure 23 that, in well 16/3-4, the chemical compaction started more-or-less at 1500 m depth, based on the P-wave velocity, whereas, in well 2/7-29, the chemical compaction started at around 3300 m depth. The red lines in Figure 23 represent a general compaction trend and the yellow lines represent the actual compaction trend that occurred due to the chemical compaction at certain depths in both the wells.
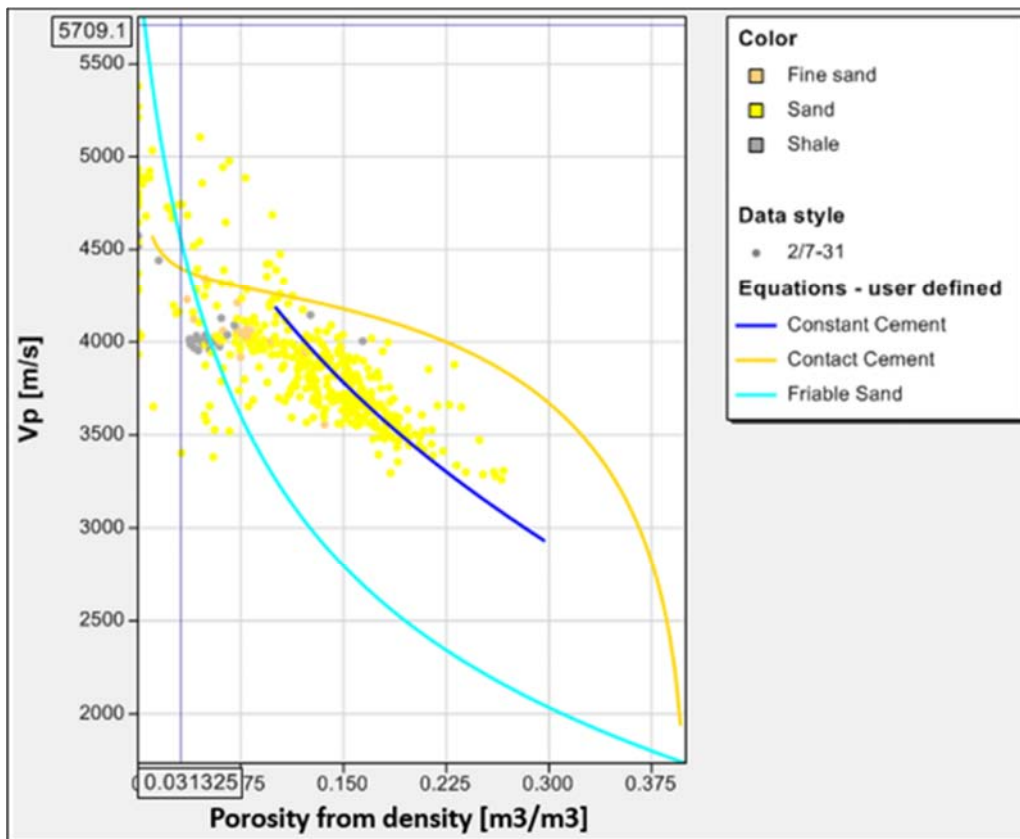
Figure 22: V_P-porosity plot of well 2/7-31 in the reservoir interval. Yellow, blue and turquoise-colored lines represent the contact cement, constant cement and friable sand models, respectively.
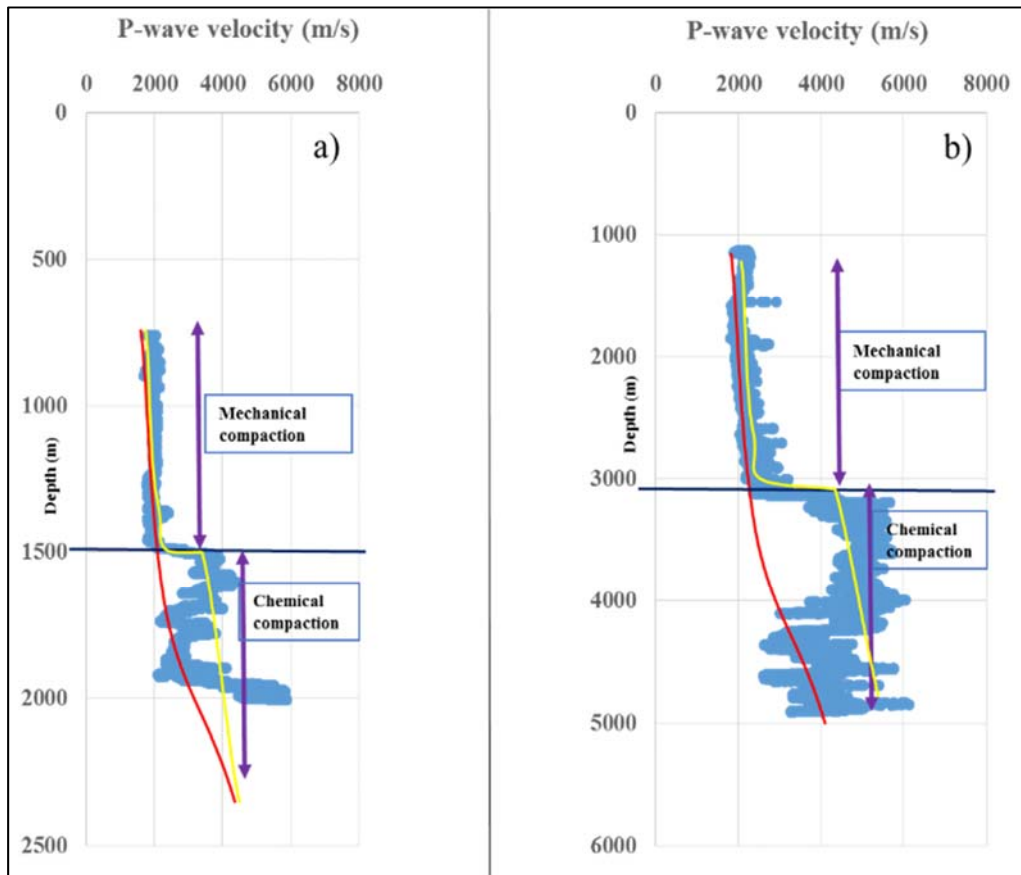
Figure 23: Rock-physics depth trends for wells 16/3-4 (a) and 2/7-29. P-wave velocities (m/s) are given on the horizontal axes and depths (m) are given on vertical axes. Red lines represent the general trend for increase in P-wave velocity with depth whereas yellow lines

5 SEISMIC INTERPRETATION

5.1 Synthetic seismograms generation

The reason for generating synthetic seismograms was to establish a relationship between well data (time and depth) and seismic data (time). In CGG-R14, synthetic analysis was done for wells 16/3-4, 16/3-5, 16/2-13 S and 16/2-16 under reverse polarity. Similarly, in MC3D-CGR2012, synthetics generated for wells included: 2/7-31, 2/7-29 and 2/7-2 under reverse polarity.

The synthetic for well 16/3-4 is shown in Figure 24. The Draupne Fm was encountered at 1914 m depth and is represented by a red (trough) event, which implies an increase in acoustic impedance inview of the reverse polarity. Basement is shown as a black reflector just below the Draupne Fm top.
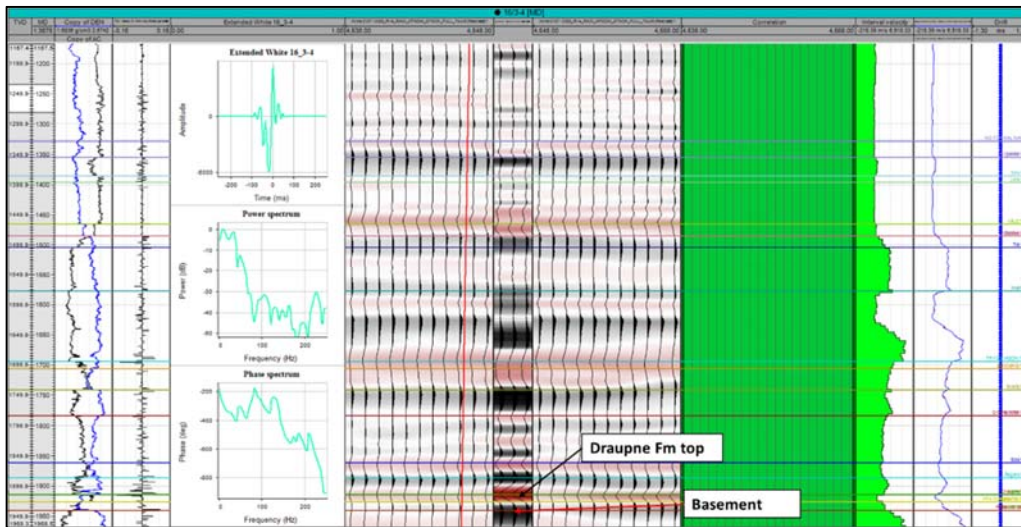
Figure 24: Synthetic profile of well 16/3-4.

In MC3D-CGR2012, taking well 2/7-29 as an example, it is observed that the Ula Fm top is indicated by a strong black reflector (peak), which means a decrease in acoustic impedance (Figure 25).
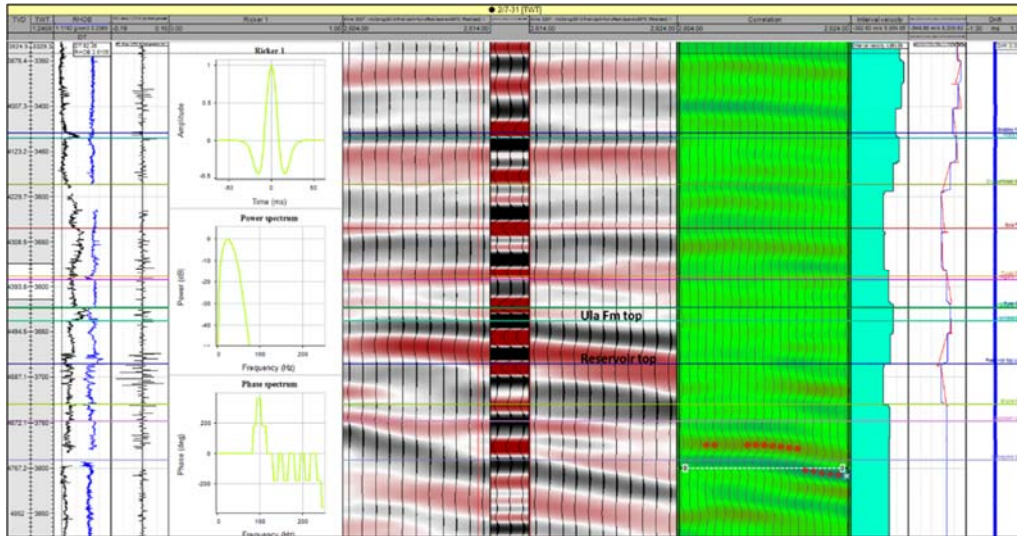
Figure 25: Synthetic profile of well 2/7-29.

5.2 Structural mapping

Several horizons were mapped to ascertain the structural evolution including: the Draupne and Ekofisk Fms in Johan Sverdrup, central North Sea (CGG-R14) and the BCU in Western Graben, southern North Sea (MC3D-CGR2012. These horizons were picked in the time domain (TWT).

Figure 26 is a time-structure contour map of the Ekofisk Fm in Johan Sverdrup. It follows a gentle trend of increasing two-way time (ms) from southeast to northwest. The shallowest part lies in the southeast and has a minimum two-way time of 1497 ms, the deepest part towards the northeast has a maximum two-way time of 1694 ms. The Ekofisk Fm is composed largely of chalk and the deposition environment was open marine with deposition of calcareous debris flows and turbidites (Skovbro, 1983).

Figure 26 is a time-structure contour map of the Draupne Fm in Johan Sverdrup. A gentle trend of increasing two-way time (ms) is observed from south to north. The time-structurally shallowest point of the Draupne Fm is measured to be at 1792 ms (TWT) and the deepest at 1964 ms (TWT). From the well logs, it is observed that the Draupne Fm is composed of shales and underlying sandstones. The Draupne sandstones are of Upper Jurassic age having unconsolidated coarse to medium-grained sands. The Draupne Fm was deposited in a marine environment and in some places it may contains sandstones that are of turbiditic origin (NPD, 2016).
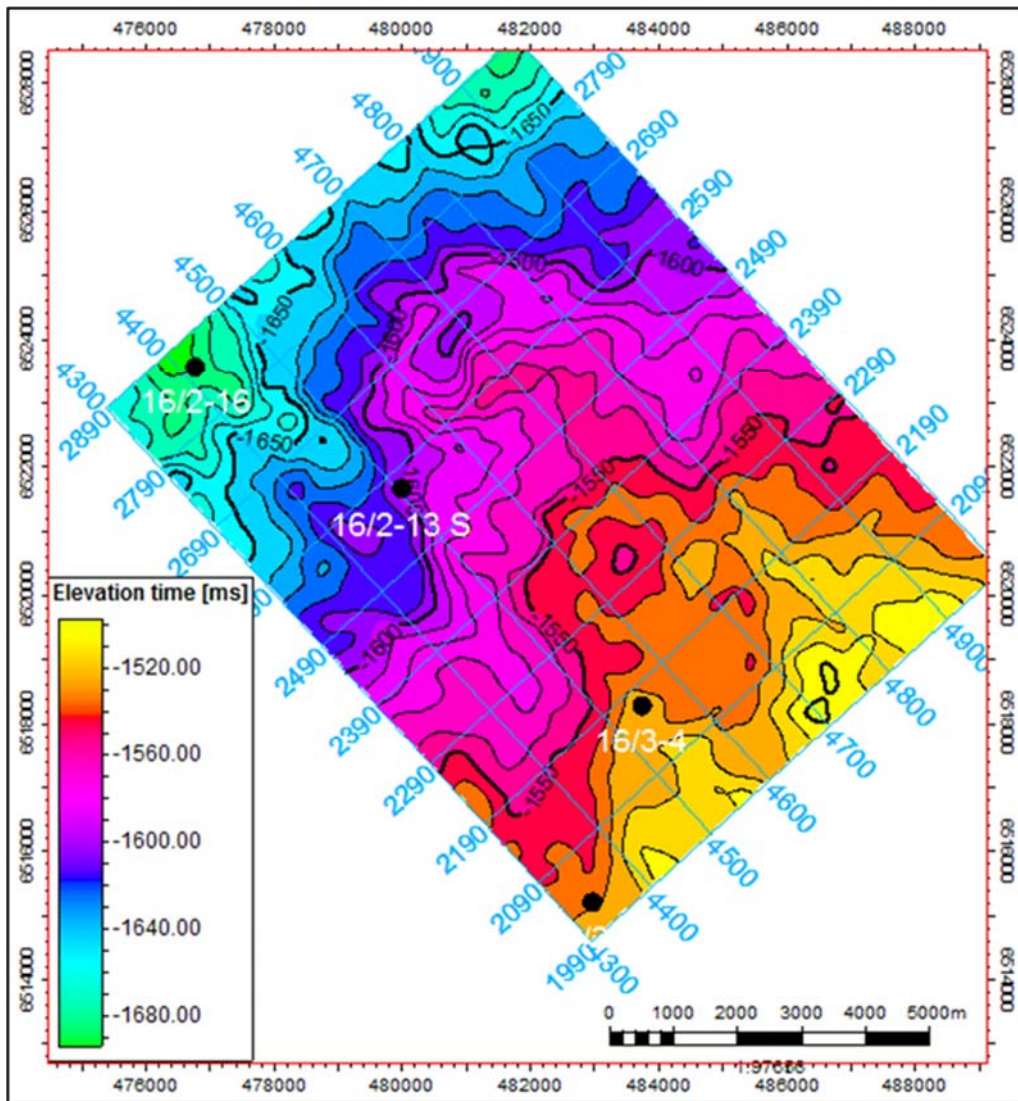
Figure 26: Time-structure contour map of the Ekofisk Fm.
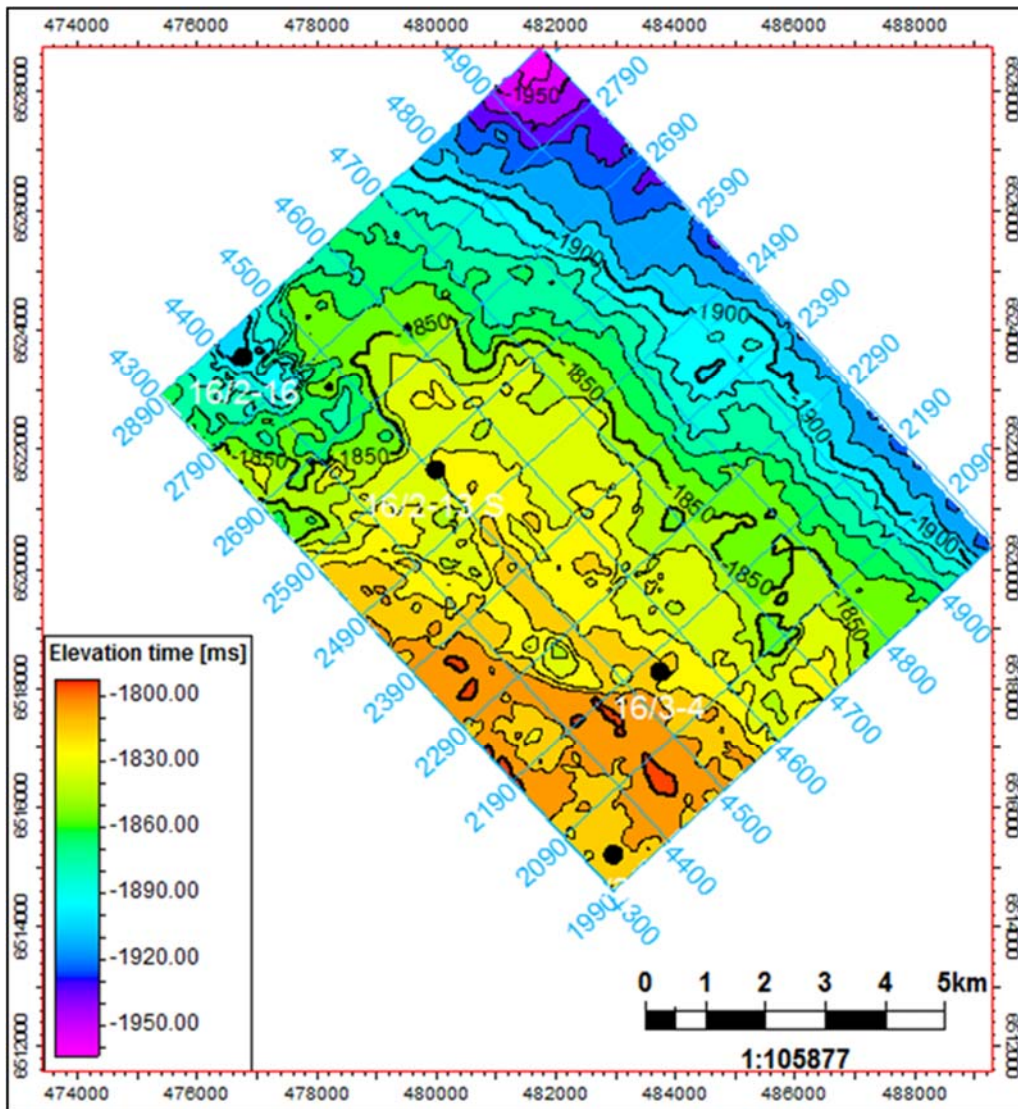
Figure 27: Time-structure contour map of the Draupne Fm.

Figure 27 is a time-structure contour map of the BCU, mapped in the Western Graben, southern North Sea. The shallowest part of the BCU is observed at 2937.94 ms (TWT) in the eastern part of the map and the deepest part at 4795 ms (TWT) in the northern part. A three-way dip closure is observed at well 2/7-31 where hydrocarbons were tested in Ula Fm sandstones.
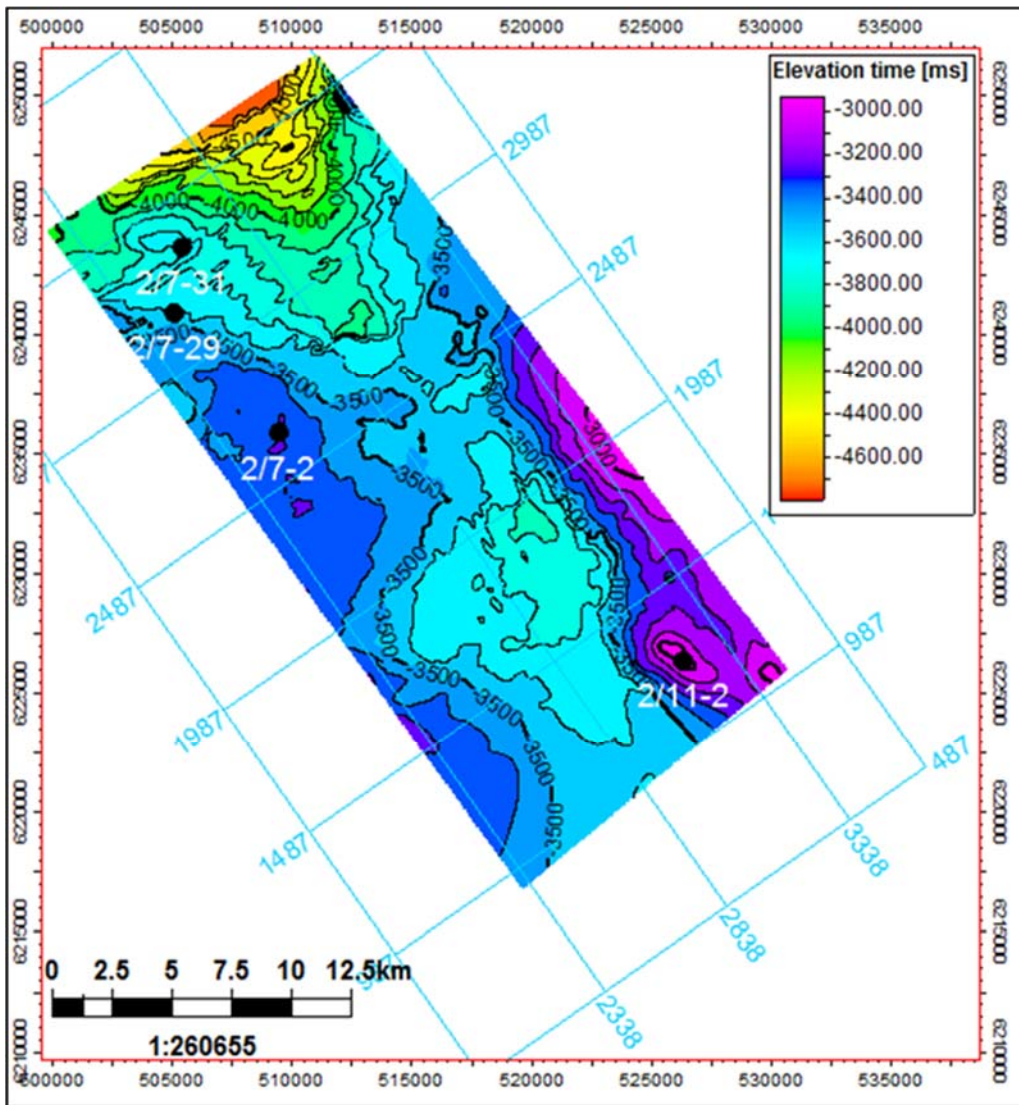
Figure 28: Time-structure contour map of the BCU.

6 LOW-FREQUENCY SPECTRAL ANALYSIS

Spectral decomposition is applied on seismic data to convert the seismic signals into their frequency components. Spectral decomposition is a seismic analysis technique that decomposes seismic data into the time-frequency domain, which often contains useful information for layer thickness estimation, stratigraphic interpretation (Puryear and Castagna, 2008), and hydrocarbon indication (Castagna et al., 2003; Sinha et al., 2005).

6.1 Spectral analysis on sections

Spectral decomposition has been applied to of the present both datasets and low-frequency analysis of known hydrocarbon-bearing zones is performed. Several sections have been observed at different frequencies (5 to 40 Hz) in order to see the anomalous response of low-frequency high-amplitude anomalies from two distinct reservoirs.

No.	Survey name	Well	Inline	Crossline	Hydrocarbon-bearing zone	
					Content	Formation
1	CGG-R14	16/3-4	2167	-	Oil	Draupne Fm
2	CGG-R14	16/3-5	2028	-	Oil	Draupne Fm
3	CGG-R14	16/2-13 S	-	4502	Oil	Draupne Fm
4	CGG-R14	16/2-16	2857	-	Oil	Draupne Fm
5	MC3D-CGR2012	2/7-31	2614	-	Oil	Ula Fm
6	MC3D-CGR2012	2/7-29	-	3182	Oil	Eldfisk Fm
7	MC3D-CGR2012	2/7-2	-	2652	Oil	Tor Fm

Table 1: Key wells and seismic lines for spectral analysis.

6.1.1 Central North Sea

Well 16/3-4 was drilled in Johan Sverdrup field, central North Sea to prove the extension of the Avaldsnes discovery to the north-east. 13.8 m of oil-saturated thick sandstones detected at a depth of 1926 m in the Intra-Draupne Fm. Figure 29 is an example of Inline 2167 from CGG-R14 (Johan Sverdrup field, central North Sea), which is spectrally decomposed into narrow bands around 10 Hz, 15 Hz and 30 Hz. The top reservoir is marked with an arrow on the low- and high-frequency spectral sections. A strong continuous high energy is observed just above the reservoir in all the spectral sections (Figure 29). However, no significant low-frequency anomaly response is observed associated with the massive homogeneous hydrocarbon-bearing sandstone of the Draupne Fm.
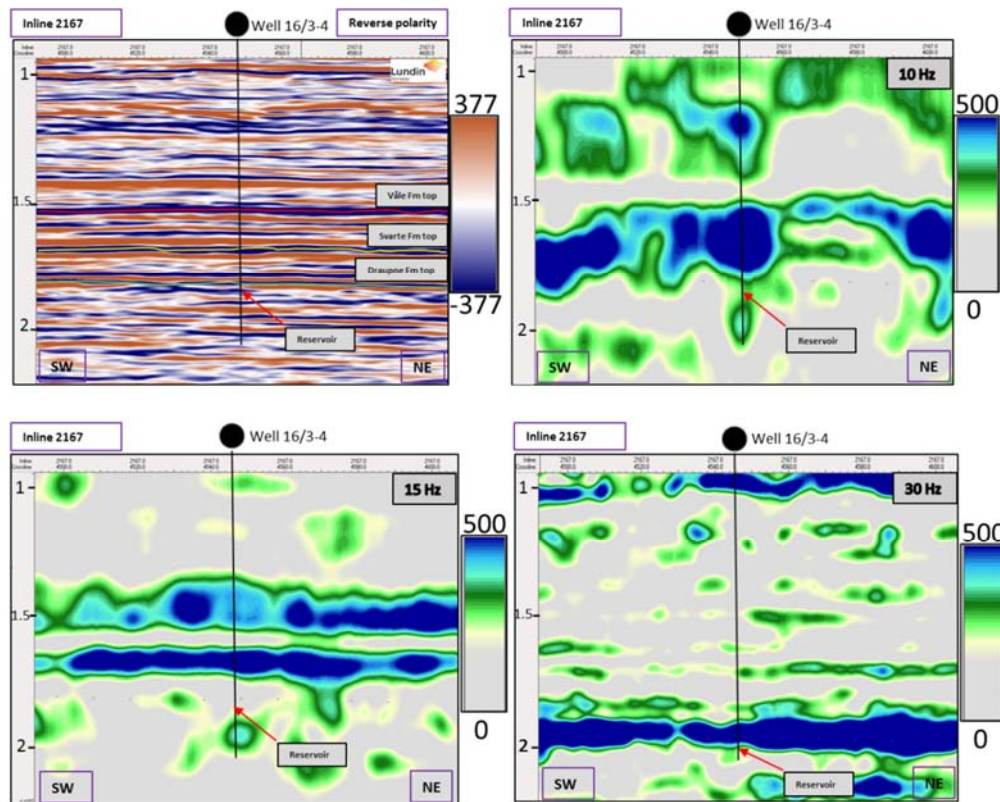
Figure 29: Inline 2167 spectral sections of 10, 15 and 30 Hz corresponding to the stacked seismic profile.

Well 16/3-5 was drilled in the Johan Sverdrup field, central North Sea, to verify the continuation of the Avaldsnes high and to test the thickness of Intra-Draupne sandstones. A 14 m thick section of oil-filled Intra-Draupne sanstones was encountered. Figure 30 is an example of inline 2028 from CGG-R14, which is spectrally decomposed to spectral sections of 7, 20 and 35 Hz. Hydrocarbons were encountered at approximately 1815 ms in the 16/3-5 well. The red arrows show the presence of oil in the reservoir. There is no low-frequency anomaly observed associated with this reservoir.
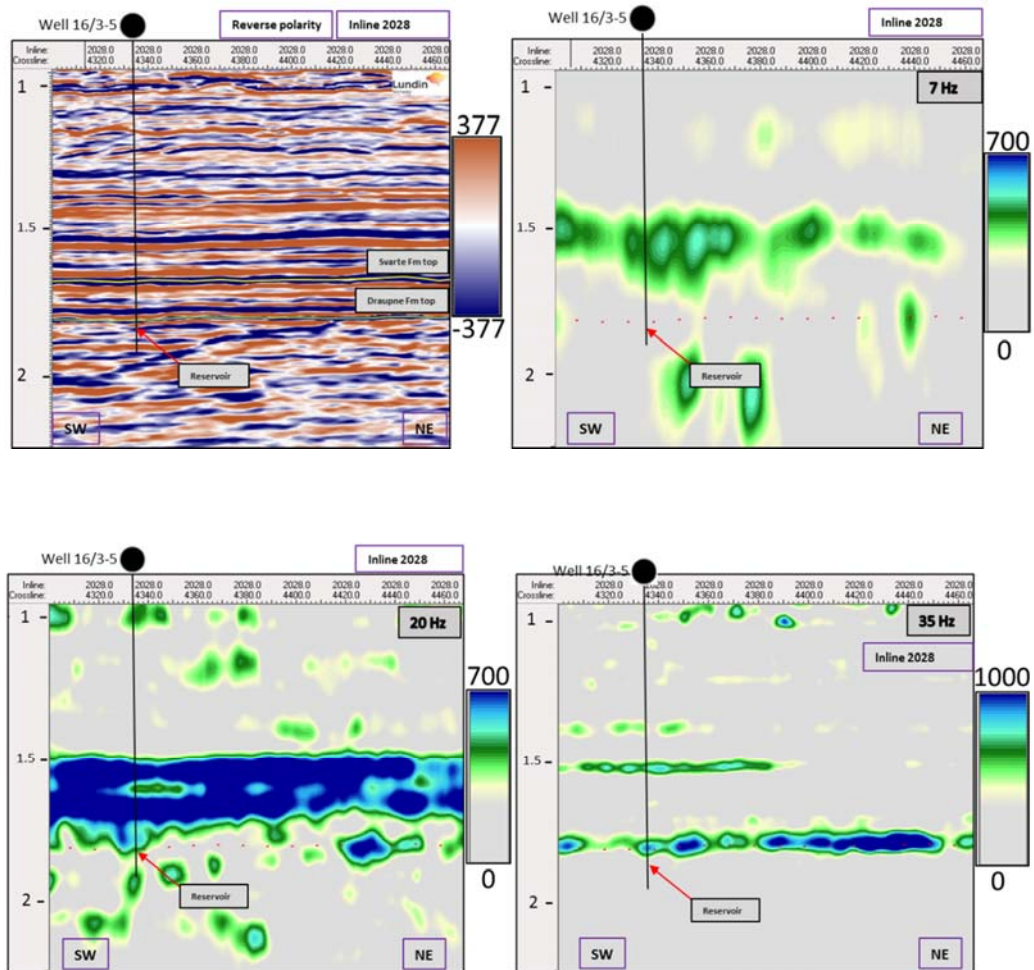
Figure 30: Inline 2028 spectral sections of 7, 20 and 35 Hz corresponding to the stacked seismic profile.

Well 16/2-13 S was aslo drilled in the Johan Sverdrup field, central North Sea, to confirm the oil-saturated sandstones of the Upper Jurassic Draupne Fm. A 25 m thick oil column was confirmed in these sandstones. Figure 31 is an example of crossline 4502 from CGG-R14, which is spectrally decomposed into narrow bands around 9 Hz, 15 Hz and 35 Hz. The oil-bearing zone was detected at 1824 ms (TWT) and the red arrow indicates the location of the oil-bearing reservoir. There are some energy anomalies observed in the 9 and 15 Hz spectral sections above the reservoir; however, no low-frequency anomalies are observed from the top or from below the reservoir.
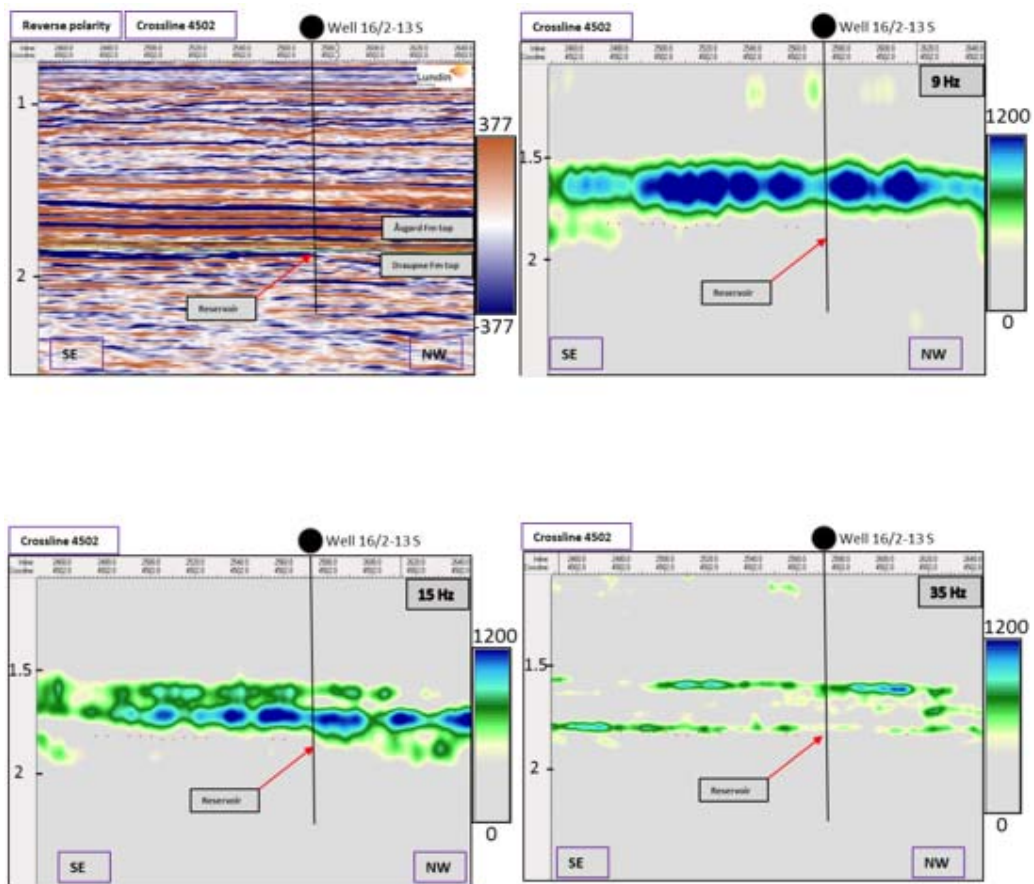
Figure 31: Crossline 4502 spectral sections of 9, 15 and 35 Hz corresponding to the stacked seismic profile.

The 16/2-16 well was drilled at Johan Sverdrup, central North Sea to acquire the information about Upper Jurassic reservoir properties (Draupne Fm). A 15 m pay zone was identified in this well. Figure 32 is an example of inline 2857 from CGG-R14 that shows the spectrally decomposed sections of inline 2857 in narrow bands around 10, 20 and 35 Hz. A strong anomaly is observed on the left side of the reservoir on the 10 Hz spectral section but it has vanished at 20 and 35 Hz. However there are not any low-frequency anomalies observed from the top or below the reservoir.
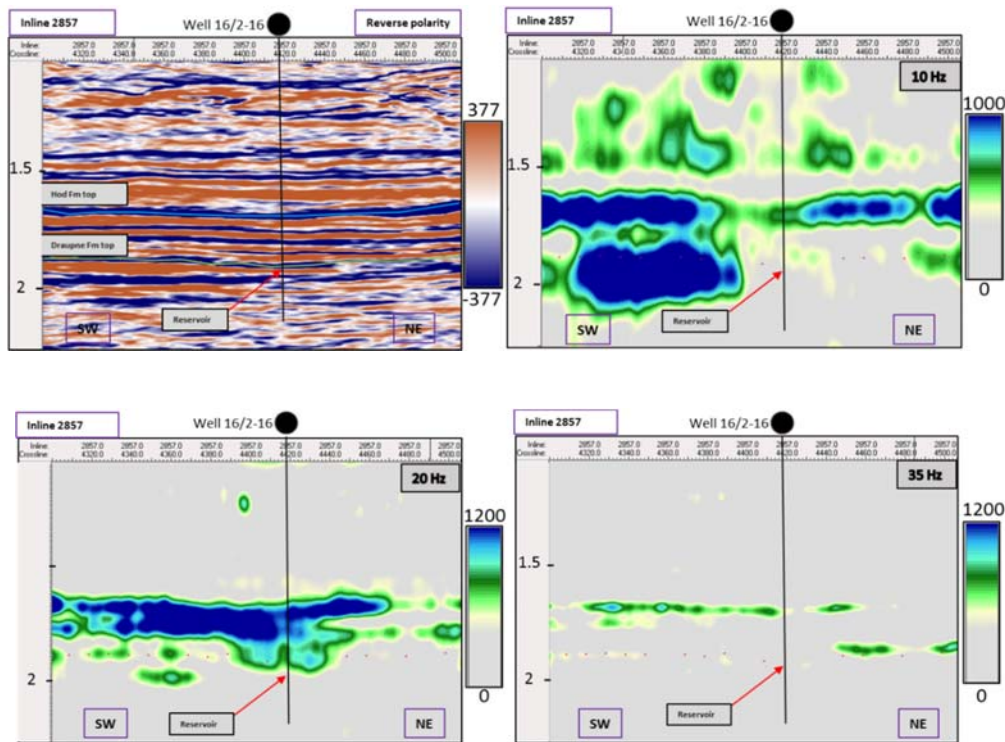
Figure 32: Inline 2857 spectral sections of 10, 20 and 35 Hz corresponding to the stacked seismic profile.

6.1.2 Southern North Sea

Well 2/7-31 was drilled in the Western Graben, southern North Sea. The main objective was to test the hydrocarbon potential of Upper Jurassic fluvial sand lenses of the Ula Fm. Hydrocarbons were encountered in the Ula sandstone at a depth of 4483.6 m. Figure 33 is an example of inline 2614, which is spectrally decomposed to narrow bands around 5, 10, 20 and 35 Hz, shown in four spectral sections. The red arrows show the hydrocarbons that were encountered at 3685 ms. A significant low-frequency anomaly associated with the reservoir is observed on the spectral sections of 5 and 10 Hz. At 20 Hz this amplitude is no longer anomalous and at 35 Hz it has nearly died out.

Well 2/7-29 was drilled in the Western Graben, southern North Sea and encountered 49 m of net sandstones of the JU2 prospect in the Eldfisk Fm. Figure 34 shows the example of crossline 3182, spectrally decomposed into sections of 5, 10, 25 and 35 Hz. Low-frequency high amplitude anomalies are observed from the top of the reservoir at 5 and 10 Hz. As the frequency of the section is increased to 25 then 35 Hz, the anomaly tends to disappear.

Well 2/7-2 was drilled in the Western Graben encountering hydrocarbons in the sandstones of the Tor Fm. Figure 35 shows crossline 2652 spectrally decomposed to spectral sections of 5, 10, 20 and 30 Hz. The reservoir is present at just about 3 s (TWT) and an amplitude anomaly is observed below the reservoir in all the spectral sections, at 5, 10, 20 and 30 Hz.
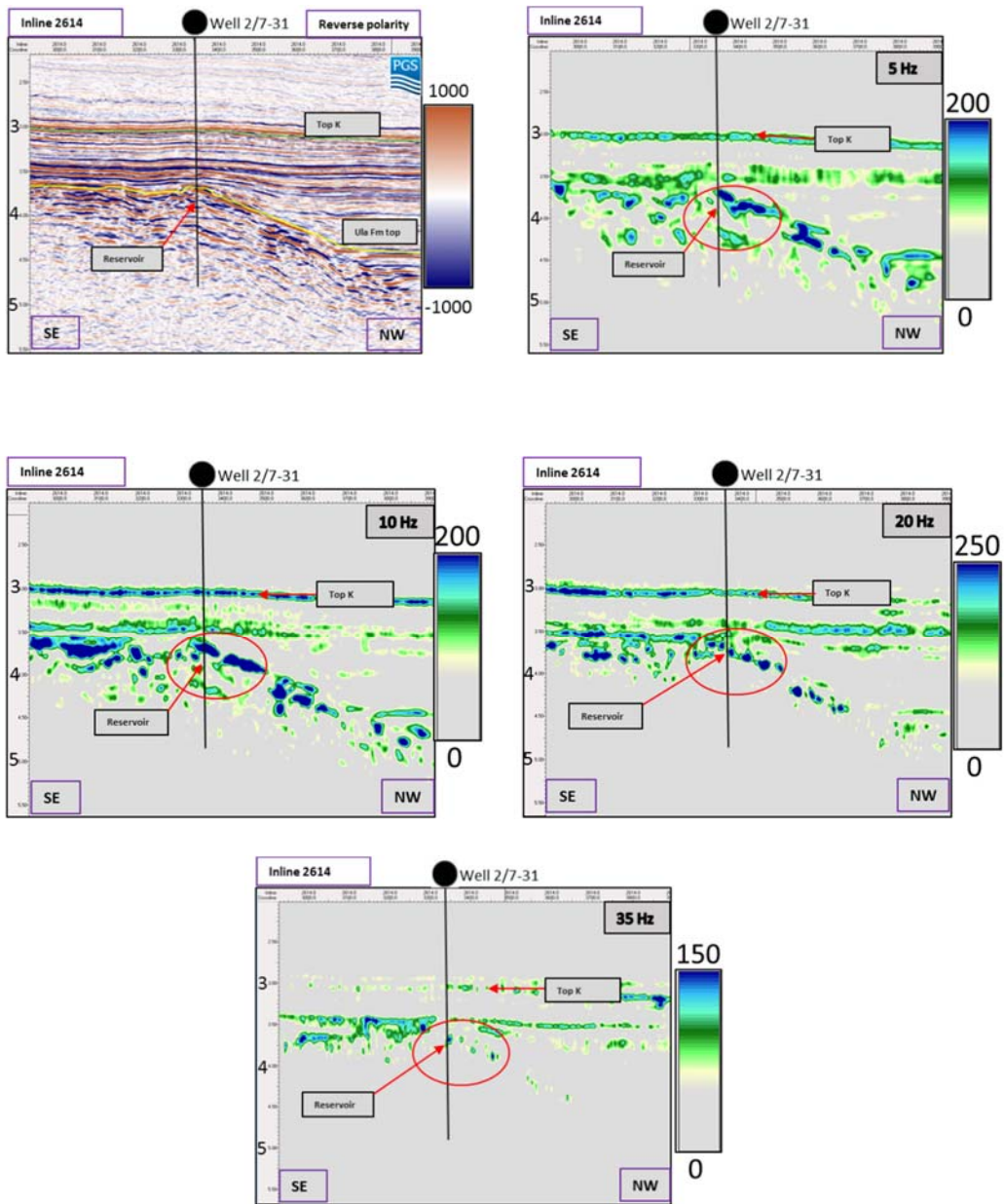
Figure 33: Inline 2614 spectral sections of 5, 10, 20 and 35 Hz corresponding to the stacked seismic profile.

47
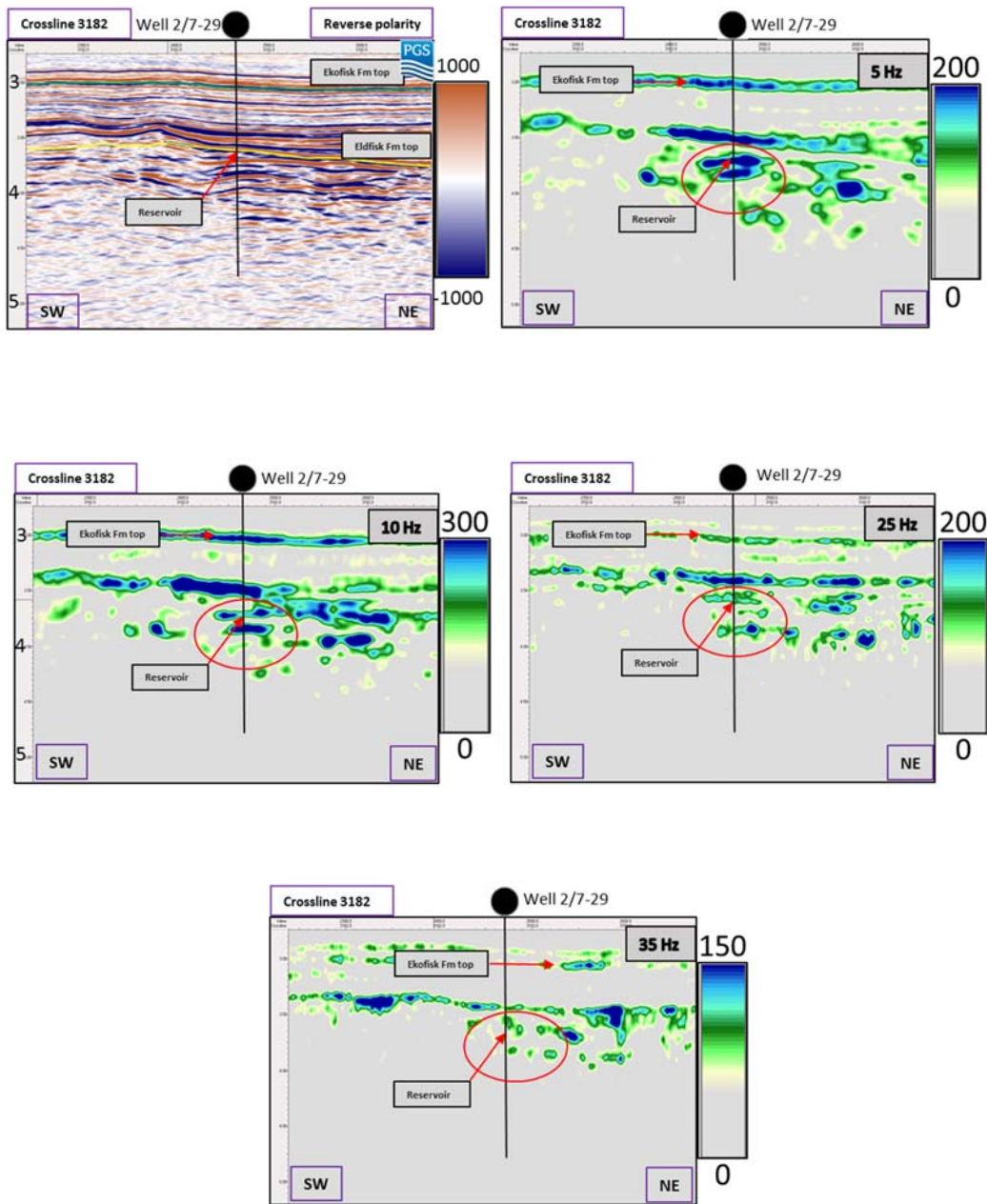
Figure 34: Crossline 3182 spectral sections of 5, 10, 25 and 35 Hz corresponding to the stacked seismic profile.
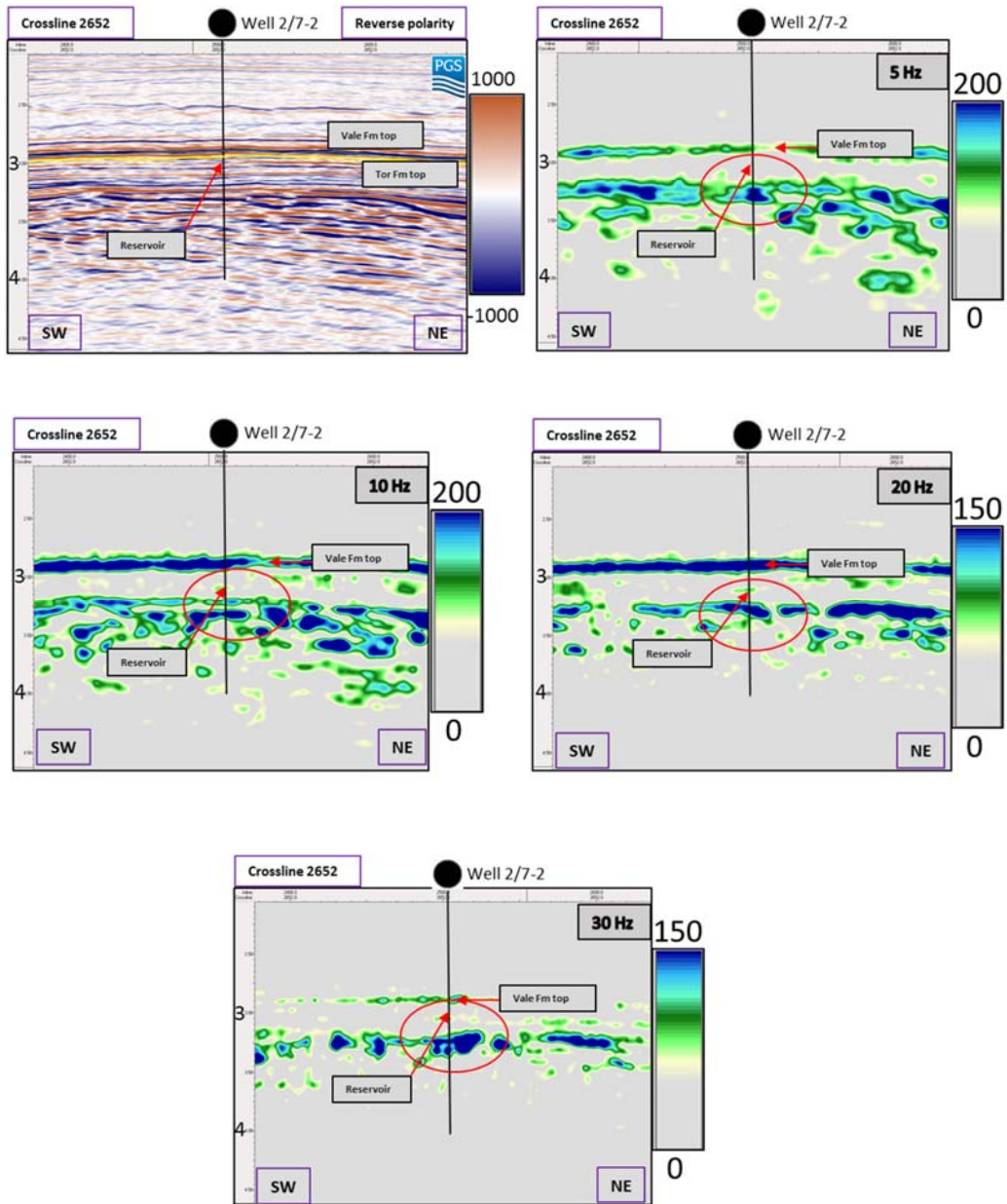
Figure 35: Crossline 2652 spectral sections of 5, 10, 20 and 30 Hz corresponding to the stacked seismic profile.

Based on the above observations, it is concluded that the low-frequency anomaly response could very often be used to indicate the presence of hydrocarbon-saturated reservoirs. However, some conditions are implied that must be considered:

1. Spectral analysis can in some cases show anomalously high-amplitude at low frequencies (about 15 or 20 Hz);

2. The anomalous response tends to disappear in high-frequency spectra (more than about 20 Hz);

3. Low-frequency anomalies may be observed from either the reservoir top or from below the reservoir; and

4. Massive thick homogeneous sandstone reservoirs may not show the low-frequency anomalous response.

6.2 Frequency-vs-time gathers

'Frequency-vs-time gathers' represent another way of visualizing seismic data as a function of amplitude versus frequency and time along the seismic trace. It can be obtained at any desired crossing points of the inlines and crosslines within a seismic cube. As a result, an ISA cube is extracted that displays the instantaneous amplitude spectrum at every two-way time along horizontal axes, with time displayed on the vertical axes. The frequencies are observed from 0 to 50 Hz. Using this method, the anomalous low-frequency response can be observed anywhere in the seismic cube.

No.	Survey name	Well	Inline	Crossline	Hydrocarbon presence	
					Content	Reservoir two way time (ms)
1	CGG-R14	16/3-4	2167	4548	Oil	1824 ms
2	CGG-R14	16/3-5	2028	4333	Oil	1815 ms
3	CGG-R14	16/2-13 S	2570	4502	Oil	1824 ms
4	CGG-R14	16/2-16	2857	4419	Oil	1862 ms
5	MC3D-CGR2012	2/7-31	2614	3337	Oil	3685 ms
6	MC3D-CGR2012	2/7-29	2461	3182	Oil	3650 ms
7	MC3D-CGR2012	2/7-2	2521	2652	Oil	2950 ms

Table 2: Frequency gathers: list of inlines and crosslines at crossing points.

6.2.1 Johan Sverdrup field, central North Sea

Figures 36, 37, 38 and 39 are plots of frequency gathers through the 16/3-4, 16/3-5, 16/2-13 S and 16/2-16 wells, respectively. The reservoir in these wells is Draupne Fm sandstones and is marked with a red-colored dashed line.

In well 16/3-4 there is no sign of any low-frequency anomaly from 0 to 50 Hz associated with the reservoir. The 16/3-5 and 16/2-13 S wells have similar low-freqeuncy reponses as 16/3-4; however, a high energy anomaly is observed from above the reservoir approximately from 10 Hz to 40 Hz. A noisy pattern of low-frequency anomaly is observed in well 16/2-16, which is observed to be similar to the overlying anomaly.
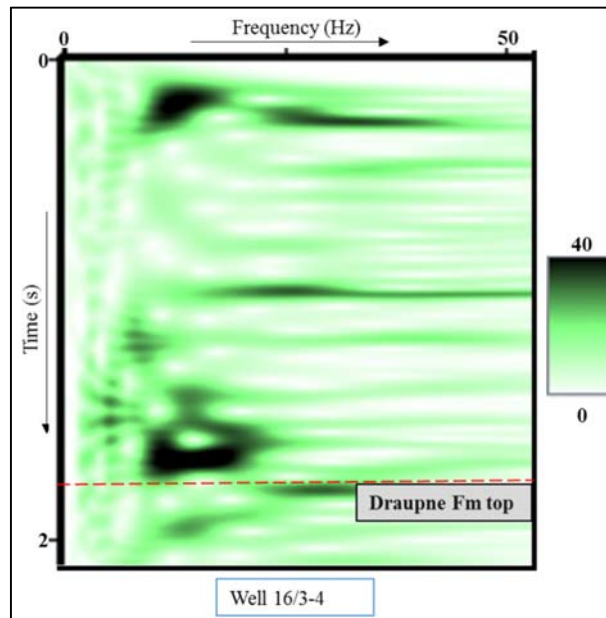

Figure 36: Frequency at well 16/3-4. The red
dashed line represents top reservoir.

Figure 37: Frequency at well 16/3-5. The red dashed
line represents top reservoir.

Figure 38: Frequency at well 16/2-13 S. The red
dashed line represents top reservoir.

Figure 39: Frequency at well 16/2-16. The red
dashed line represents top reservoir.

6.2.2 Western Graben, southern North Sea

Figures 40, 41 and 42 are frequency gathers, showing amplitude spectra at each time sample of single seismic trace through wells 2/7-31, 2/7-29 and 2/7-2, respectively.

In Figure 40, the reservoir consists of sand lenses of the Ula Fm (marked with a red dashed line) at 3.685 s (TWT). A strong amplitude anomaly at the reservoir is oberserved at low frequencies, ranging from about 5 to 15 Hz.

In Figure 41, the reservoir is made up of sandstones of the Eldfisk Fm (marked with red dashed line) at 3.650 s (TWT). A more diffuse amplitude anomaly than in Figure 40 is observed at reservoir depths here, roughly from 5 to 20 Hz.

In Figure 42, the reservoir consists of sandstones of the Tor Fm at 2.95 s (TWT). A very diffuse low-frequency anomaly ranging from 7 Hz to 25 Hz is observed. However, at somewhat greater depth amplitudes concentrate at low frequencies of about 5 to 15 Hz, which looks a lot like a so-called 'shadow' beneath the reservoir.

The above observations indicate that low-frequency analysis can be a significant tool to indicate the presence of hydrocarbons in the subsurface. However, no convincing sign of low-frequency anomalies have been observed from the massive thick sandstone reservoir of Draupne Fm in Johan Sverdrup field, southern North Sea. But, reservoirs of sandstones with thin successions of silty-sand from Ula Fm, Eldfisk Fm and Tor Fm in Western Graben, southern North Sea responded with significant low frequencies anomalies (<20 Hz) associated with hydrocarbon filled reservoirs.
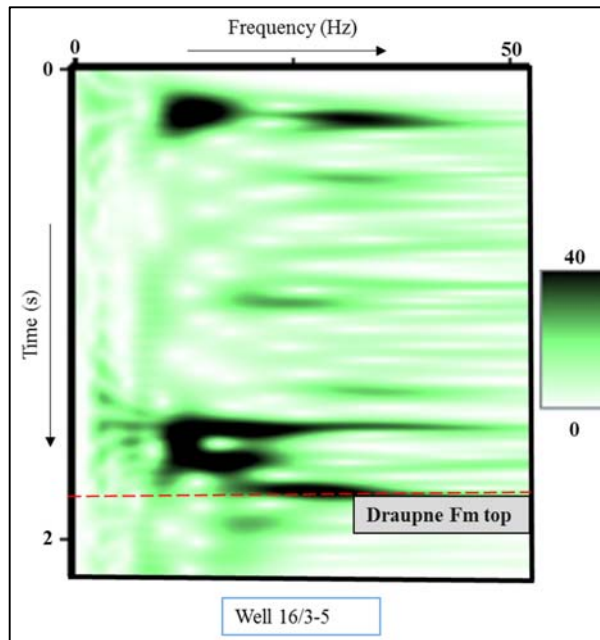
Figure 41: Frequency at well 2/7-29. The red dashed line represents top reservoir.

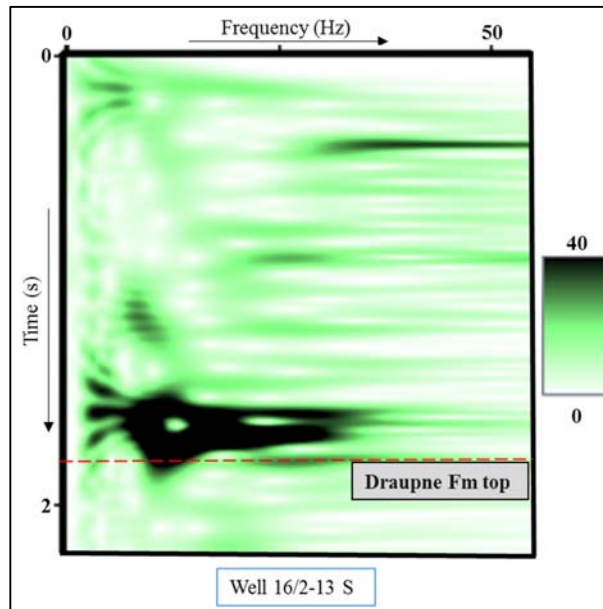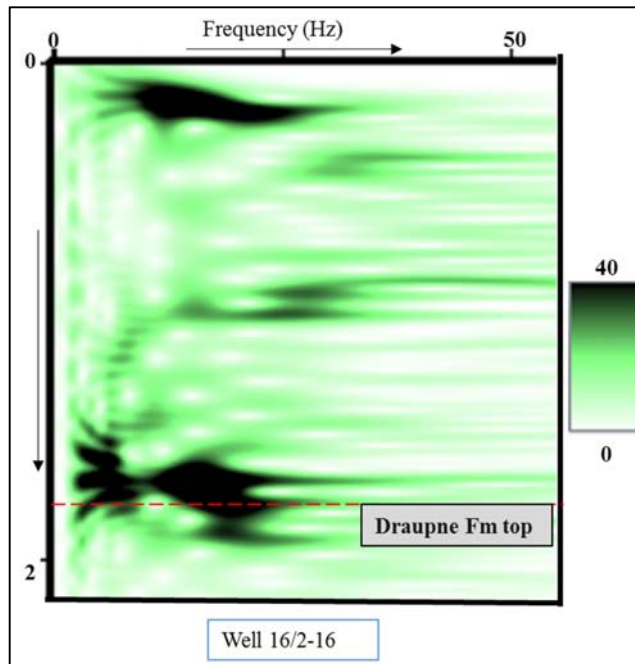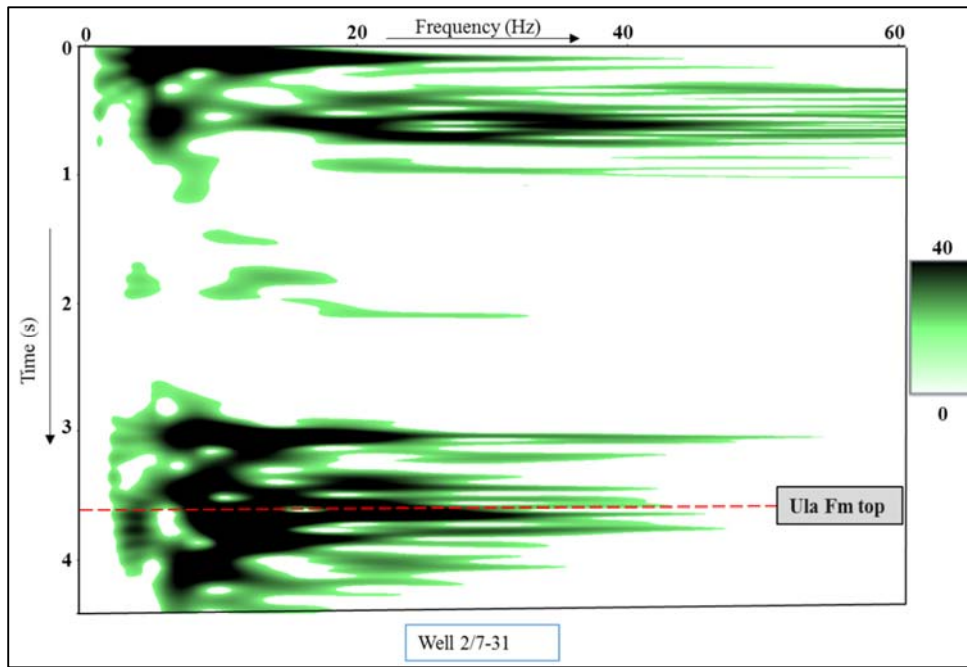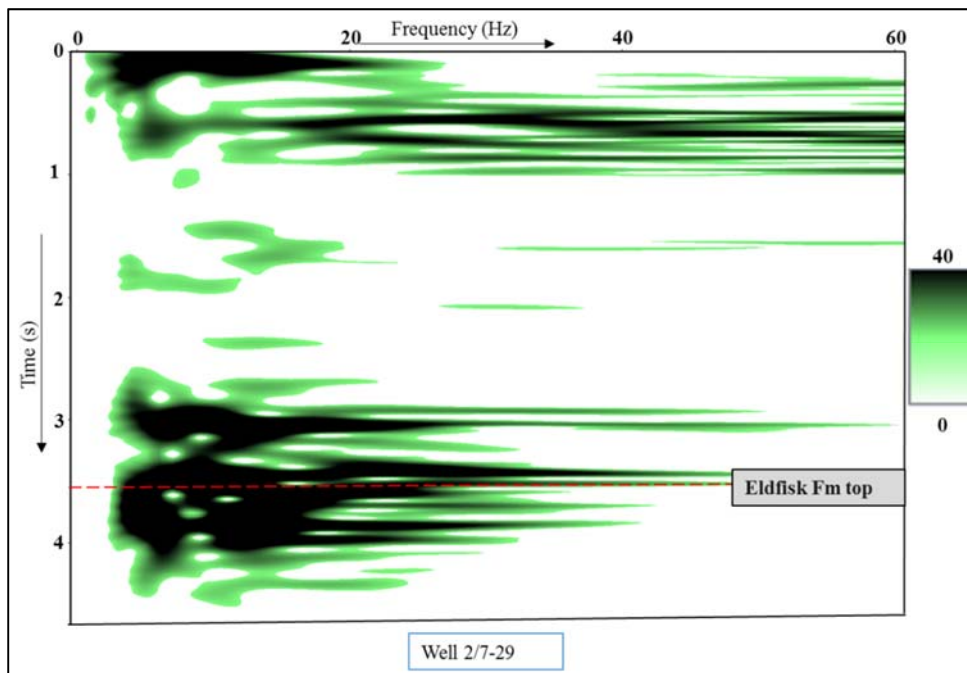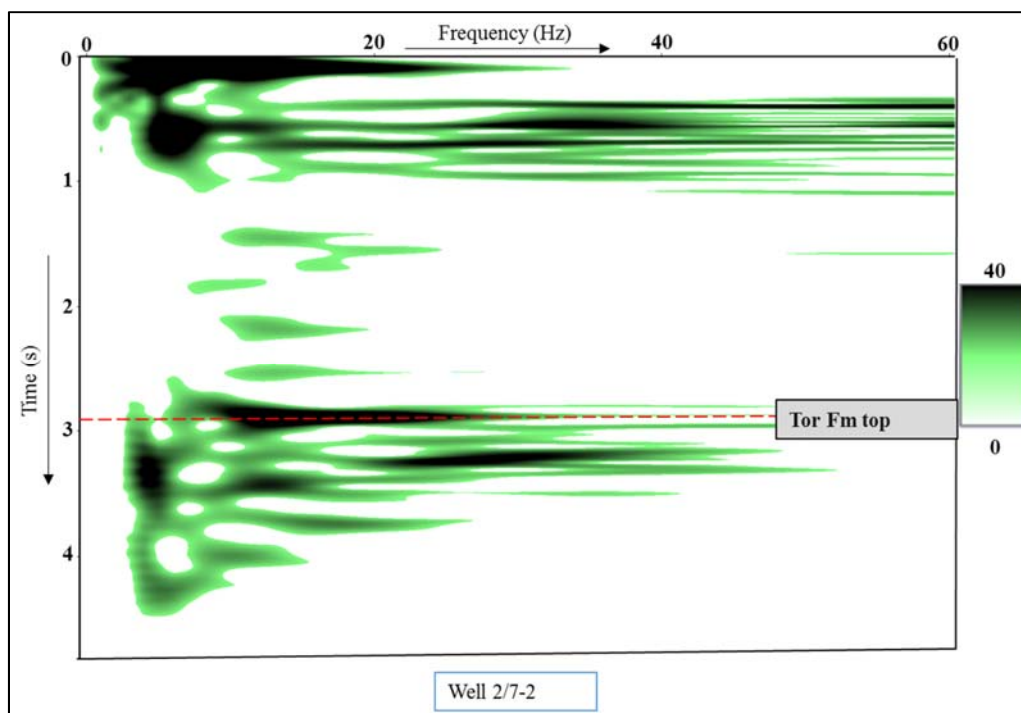Figure 40: Frequency at well 2/7-31. The red dashed line represents top reservoir.

Figure 42: Frequency at well 2/7-2. The red dashed line represents top reservoir.

7 DISCUSSIONS AND CONCLUSIONS

In this study, we have observed two different types of reservoir having different lithological properties. Based on the critical well analysis, we have concluded that the Draupne Fm reservoir from the Johan Sverdrup field, central North Sea, consists of thick massive homogeneous sandstone, as it shows a smooth trend in the gamma-ray log response. On the other hand, the Ula Fm reservoir in the Western Graben, southern North Sea, consists of sand lenses; so the Ula reservoir could be termed a heterogeneous reservoir. Eldfisk and Tor reservoirs from the Western Graben showed similar lithological reservoir properties as the Ula reservoir.

V_P-vs-porosity plots are a useful tool for determining reservoir properties. In this study, we compared the results of V_P-vs- porosity plots between two reservoirs, i.e. the Ula and Draupne reservoirs. It is observed that the Draupne Fm reservoir plotted near to the contact-cement model; thus is was inferred to consist of well-sorted grains and to have higher porosities. However, the Ula Fm reservoir plotted along the constant-cement model. Reduction in porosities in the Ula Fm is deemed to be due to the comparatively poor sorting of grains as those in the Draupne Fm that led to reduced porosities down to about 12 %. Therefore, it is concluded that grains in the Draupne Fm reservoir are well-sorted and typify the homogeneity of the reservoir.

Spectral decomposition was applied to the seismic data to acquire the frequency components of seismic signals. Low-frequency high-amplitude anomalies were searched for which could be associated with hydrocarbon-bearing reservoirs. These anomalies could appear in the frequency range of 5 to 20 Hz either at or below the reservoir. Below the reservoir, however, the anomalous response of amplitudes associated with a hydrocarbon-saturated reservoir tends to disappear on higher frequency profiles (>20 Hz). This mechanism is so called amplitude attenuation that can be used to identify the hydrocarbons.

Based on our analysis, the low-frequency anomalous response is found to be strong at and below the interbedded heterogeneous Ula, Eldfisk and Tor reservoirs, but the response was more diffuse at and below the massive homogeneous Draupne reservoir at Johan Sverdrup. However, an anomalous low-frequency response was observed above the Draupne Fm reservoir, due to the properties of overlying formations

and boundaries. These results seem to support the hypothesis proposed by Goloshubin and Chabyshova (2012), according to which, low-frequency anomalies associated with hydrocarbons are expected to be weakest in massive homogeneous thick reservoirs and strongest for highly interbedded pearmeable reservoirs.

This suggests that the relatively heterogeneous nature of the Ula, Eldfisk and Tor reservoirs and their relatively low permeability (though quite high, but not nearly as permeable as the Draupne reservoir) lead to greater attenuation of the high-frequency content there (Western Graben) than at Johan Sverdrup. However, such a mechanism needs further investigation and other factors, like e.g. resonance effects due to conversions at reservoir interfaces involving fast-slow-fast P-waves (Ferrazzini & Aki, 1987; Chabyshova & Goloshubin, 2014) could also be a contributing element.

8 REFERENCES

Ahmad, S. S., R. J. Brown, and A. Escalona, 2016, Frequency-dependent velocity analysis and offset-dependent low-frequency anomalies from hydrocarbon-filled reservoirs: Presented at the 78th EAGE Conference & Exhibition.

Ahmadi, Z., M. Sawyers, S. Kenyon-Roberts, C. Stanworth, K. Kugler, J. Kristensen, E. Fugelli, E. D. Paleocene, C. Graham, and A. Armour, 2003, The Millennium Atlas: petroleum geology of the central and northern North Sea: The Geological Society of London, London, 235-259.

Avseth, P., 2012, Using rock physics to reduce seismic exploration risk on the Norwegian shelf: Presented to Geoforskning.no, 22nd May, 2012; posted at http://geoforskning.no/foredrag/oljeoggass/190-kanbergartsfysikkbidra.

Avseth, P., T. Mukerji, and G. Mavko, 2010, Quantitative seismic interpretation: Applying rock physics tools to reduce interpretation risk: Cambridge University Press.

Batzle, M. L., D.-H. Han, and R. Hofmann, 2006, Fluid mobility and frequency-dependent seismic velocity – Direct measurements: Geophysics, **71**, N1-N9.

Blystad, P., 1995, Structural Elements of the Norwegian Continental Shelf: The Norweigan Sea Region: Norwegian Petroleum Directorate.

Brasher, J., and K. Vagle, 1996, Influence of lithofacies and diagenesis on Norwegian North Sea chalk reservoirs: AAPG bulletin, **80**, 746-768.

Brekke, H., 2000, The tectonic evolution of the Norwegian Sea continental margin, with emphasis on the Voring and More basins: Special Publication - Geological Society of London, **167**, 327-378.

Carcione, J. M., C. Morency, and J. E. Santos, 2010, Computational poroelasticity – A review: Geophysics, **75**, 75A229-275A243.

Casey, B., R. Romani, and R. Schmitt, Year, Appraisal geology of the Saltire Field, Witch Ground Graben, North Sea: Geological Society, London, Petroleum Geology Conference series, Geological Society of London, 507-517.

Castagna, J. P., and S. Sun, 2006, Comparison of spectral decomposition methods: First break, **24**.

Castagna, J. P., S. Sun, and R. W. Siegfried, 2003, Instantaneous spectral analysis: Detection of low-frequency shadows associated with hydrocarbons: The Leading Edge, **22**, 120-127.

Chabyshova, E., and G. Goloshubin, 2014, Seismic modeling of low-frequency "shadows" beneath gas reservoirs: Geophysics, **79**, D417-D423.

Chakraborty, A., and D. Okaya, 1995, Frequency-time decomposition of seismic data using wavelet-based methods: Geophysics, **60**, 1906-1916.

Chen, X.-H., Z.-H. He, S.-X. Zhu, W. Liu, and W.-L. Zhong, 2012, Seismic low-frequency-based calculation of reservoir fluid mobility and its applications: Applied Geophysics, **9**, 326-332.

Cohen, K., S. Finney, and P. Gibbard, 2013, International chronostratigraphic chart 2013/01. International Commission on Stratigraphy.

Deegan, C. t., and B. J. Scull, 1977, A standard lithostratigraphic nomenclature for the Central and Northern North Sea: Her Majesty's Stationery Office.

Dvorkin, J., and A. Nur, 1996, Elasticity of high-porosity sandstones: Theory for two North Sea data sets: Geophysics, **61**, 1363-1370.

Fanka, W. R. T., 2012, Well Log and Seismic Data Interpretation: MSc thesis, Norwegian University of Science and Technology, 77 pp.

Ferrazzini, V., and K. Aki, 1987, Slow waves trapped in a fluid-filled infinite crack: implication for volcanic tremor: Journal of Geophysical Research: **92**, 9215-9223.

Gennaro, M., J. Wonham, R. Gawthorpe, and G. Sælen, 2013, Seismic stratigraphy of the Chalk Group in the Norwegian Central Graben, North Sea: Marine and Petroleum Geology, **45**, 236-266.

Gołędowski, B., S. B. Nielsen, and O. R. Clausen, 2012, Patterns of Cenozoic sediment flux from western Scandinavia: Basin Research, **24**, 377-400.

Goloshubin, G., and E. Chabyshova, 2012, A possible explanation of low frequency shadows beneath gas reservoirs: 82nd SEG Annual Meeting, Society of Exploration Geophysicists.

Goloshubin, G., C. Van Schuyver, V. Korneev, D. Silin, and V. Vingalov, 2006, Reservoir imaging using low frequencies of seismic reflections: The Leading Edge, **25**, 527-531.

Goloshubin, G. M., V. A. Korneev, and V. M. Vingalov, 2002, Seismic low-frequency effects from oil-saturated reservoir zones: 72nd SEG Annual Meeting, Society of Exploration Geophysicists.

Herrington, P., K. Pederstad, and J. Dickson, 1991, Sedimentology and diagenesis of resedimented and rhythmically bedded chalks from the Eldfisk field, North Sea Central Graben: AAPG Bulletin, **75**, 1661-1674.

Hossain, Z., and L. MacGregor, 2014, Advanced rock-physics diagnostic analysis: A new method for cement quantification: The Leading Edge, **33**, 310-316.

Huang, L., N. Dyaur, and R. R. Stewart, 2015, Elastic properties of 3D-printed physical models: Fluid substitution observations in cracked media: 85th SEG Annual Meeting, Society of Exploration Geophysicists.

Jackson, C. A., K. E. Kane, and E. Larsen, 2010, Structural evolution of minibasins on the Utsira High, northern North Sea; implications for Jurassic sediment dispersal and reservoir distribution: Petroleum Geoscience, **16**, 105-120.

Jenyon, M. K., 1985, Basin-edge diapirism and updip salt flow in Zechstein of southern North Sea: AAPG Bulletin, **69**, 53-64.

Lee, M., and Y. Hwang, Year, Tectonic evolution and structural styles of the East Shetland Basin: Geological Society, London, Petroleum Geology Conference series, Geological Society of London, 1137-1149.

Lefeuve-Mesgouez, G., A. Mesgouez, G. Chiavassa, and B. Lombard, 2012, Semi-analytical and numerical methods for computing transient waves in 2D acoustic/poroelastic stratified media: Wave Motion, **49**, 667-680.

Lu, W., and F. Li, 2013, Seismic spectral decomposition using deconvolutive short-time Fourier transform spectrogram: Geophysics, **78**, V43-V51.

Madonna, C., N. Tisato, S. Boutareaud, and D. Mainprice, 2010, A new laboratory system for the measurement of low frequency seismic attenuation: 80th SEG Annual Meeting, Society of Exploration Geophysicists.

Mallat, S. G., and Z. Zhang, 1993, Matching pursuits with time-frequency dictionaries: Signal Processing, IEEE Transactions on signal processing, **41**, 3397-3415.

Mosar, J., 2003, Scandinavia's North Atlantic passive margin: Journal of Geophysical Research: Solid Earth, **108 (B8)**, 2360.

Müller, B., M. L. Zoback, K. Fuchs, L. Mastin, S. Gregersen, N. Pavoni, O. Stephansson, and C. Ljunggren, 1992, Regional patterns of tectonic stress in Europe: Journal of Geophysical Research: Solid Earth, **97**, 11783-11803.

Nakagawa, S., S. Nakashima, and V. A. Korneev, 2016, Laboratory measurements of guided-wave propagation within a fluid-saturated fracture: Geophysical Prospecting, **64**, 143-156.

NPD (2016). FactPages. 2014, from http://www.npd.no. Seen on 30 May 2016.

Okaya, D. A., E. Karageorgi, T. V. McEvilly, and P. E. Malin, 1992, Removing vibrator-induced correlation artifacts by filtering in frequency-uncorrelated time space: Geophysics, **57**, 916-926.

Partyka, G., J. Gridley, and J. Lopez, 1999, Interpretational applications of spectral decomposition in reservoir characterization: The Leading Edge, **18**, 353-360.

Puryear, C. I., and J. P. Castagna, 2008, Layer-thickness determination and stratigraphic interpretation using spectral inversion: Theory and application: Geophysics, **73**, R37-R48.

Qian, S., and D. Chen, 1994, Signal representation using adaptive normalized Gaussian functions: Signal processing, **36**, 1-11.

Rossland, A., A. Escalona, and R. Rolfsen, 2013, Permian–Holocene tectonostratigraphic evolution of the Mandal High, Central Graben, North Sea: AAPG Bulletin, **97**, 923-957.

Silin, D., and G. Goloshubin, 2010, An asymptotic model of seismic reflection from a permeable layer: Transport in Porous Media, **83**, 233-256.

Sinha, S., P. S. Routh, P. D. Anno, and J. P. Castagna, 2005, Spectral decomposition of seismic data with continuous-wavelet transform: Geophysics, **70**, P19-P25.

Skovbro, B., 1983, Depositional conditions during chalk sedimentation in the Ekofisk area Norwegian North Sea, Petroleum Geology of the Southeastern North Sea and the Adjacent Onshore Areas: Springer, 169-175.

Stockwell, R. G., L. Mansinha, and R. Lowe, 1996, Localization of the complex spectrum: the S transform: Signal Processing, IEEE Transactions on signal processing, **44**, 998-1001.

Sørlie, R., E. Hammer, M. Charnock, H. Amundsen, and L. Riber, 2012, Integrated geological studies as a key to understanding the geology of the Johan Sverdrup discovery – with examples from the PL 501 area: FORCE Seminar Abstracts, Jurassic and Lower Cretaceous Sedimentary Systems of the Utsira High, Norwegian Petroleum Directorate.

Tai, S., C. Puryear, and J. P. Castagna, 2009, Local frequency as a direct hydrocarbon indicator: 79th SEG Annual Meeting, Society of Exploration Geophysicists.

Taner, M. T., F. Koehler, and R. E. Sheriff, 1979, Complex seismic trace analysis: Geophysics, **44**, 1041-1063.

Wilson, R. W., K. J. W. McCaffrey, R. E. Holdsworth, J. Imber, R. R. Jones, A. I. F. Welbon, and D. Roberts, 2006, Complex fault patterns, transtension and structural segmentation of the Lofoten Ridge, Norwegian margin: Using digital mapping to link onshore and offshore geology: Tectonics, **25**, TC4018.

Zhong, X., 2014, Low-frequency reflection seismic and direct hydrocarbon indication: MSc thesis, University of Stavanger, 65 pp.